Chitosan stimulates root hair callose deposition and inhibits root hair growth

Matěj Drs[1,2], Samuel Haluška[1,2], Eliška Škrabálková[1,2], Pavel Krupař[2], Andrea Potocká[1], Lucie Brejšková[1], Karel Muller[1], Natalia Serrano[1], Aline Voxeur[3], Samantha Vernhettes[3], Jitka Ortmannová[1], George Caldarescu[2], Matyáš Fendrych[2], Martin Potocký[1], Viktor Žárský[1,2], Tamara Pečenková[1,2*]

[1] Institute of Experimental Botany of the Czech Academy of Sciences, Rozvojová 263, 165 02, Prague 6, Czech Republic

[2] Department of Experimental Plant Biology, Faculty of Science, Charles University, Viničná 5, 128 44, Prague 2, Czech Republic

[3] Université Paris-Saclay, INRAE, AgroParisTech, Institut Jean-Pierre Bourgin (IJPB), 78000, Versailles, France

*corresponding author pecenkova@ueb.cas.cz

Abstract

Although angiosperm plants have a general capacity to react after the immunity elicitor chitin or chitosan treatment by the cell wall callose deposition, this response in particular cell types and its evolutionary conservation is not understood. Here we show that also the growing root hairs (RHs) of Arabidopsis can respond to a mild (0.001%) chitosan treatment by the callose deposition and by a deceleration of the RH growth. We demonstrate that the glucan synthase-like 5 (GSL5)/PMR4 is vital for chitosan-induced callose deposition but not for RH growth inhibition. Upon the higher chitosan concentration (0.01%) treatment, RHs do not deposit callose, while growth inhibition is prominent. To understand the specificities of the low and high concentration chitosan treatments, we analysed the corresponding PTI signalling components, gene expression, and RH cellular endomembrane and cytoskeleton modifications. Importantly, chitosan-induced callose deposition is also present in the functionally analogous and evolutionarily only distantly related RH-like structures rhizophores (lycophytes) and rhizoids (bryophytes). Our results point to the RH callose deposition as a conserved strategy of soil-anchoring plant cells (rhizoids/rhizophores/RHs) to deal with mild biotic stress. At the same time, high chitosan concentration prominently disturbs intracellular dynamics, tip-localised endomembrane compartments and RH growth, precluding callose deposition.

Introduction

Root hairs (RHs) are unicellular plant structures crucial for several aspects of root function: mechanical anchorage of a plant in a substrate, the absorption of water and essential nutrients due to increased root surface, and in root-microbe interactions. In the model plant *Arabidopsis thaliana*, RH cell fate is determined by a position-dependent signalling cascade governed by specific transcription factors, leading to the RH initiation, bulging and cylindrical/polarised tip growth (Carol and Dolan, 2002; Dolan, 1996; Parker et al., 2000; Vissenberg et al., 2020). Several root hair-defective (RHD) genes, F-actin cytoskeletal meshwork and secretory pathway play a prominent role in this process (Baluška et al., 2000; Ichikawa et al., 2014). The tip growth is supported by constant modification of the preexisting cell wall (CW), as documented by the vital importance of several cellulose and hemicellulose biosynthesis participants (Cavalier et al., 2008; Park et al., 2011).

In aerial plant parts, when a pathogen attacks the plant cell, pathogen-associated molecular patterns (PAMP) triggered immunity (PTI) and potentially effector-triggered immunity (ETI) are activated (Jones and Dangl, 2006; Ngou et al., 2021). One of the earliest defence responses to a pathogen attack is the deposition of β-1,3 glucan polysaccharide callose by which the plant reinforces cell walls and blocks the pathogen entry (Jacobs et al., 2003). In Arabidopsis, among 12 callose synthase genes, only one of them, *GSL5* or *PMR4* (*POWDERY MILDEW RESISTANT 4*), is expressed upon pathogenic infection or elicitor treatment, such as fungal cell wall derived chitin and chitosan, but also endogenous damage-associated patterns (DAMP) (Denoux et al., 2008; Gómez-Gómez et al., 1999; Luna et al., 2011; Verma and Hong, 2001; Vogel and Somerville, 2000).

In contrast to shoots, the roots are constantly exposed to a mixture of microorganisms, and plants need to prevent the over-activation of immunity in roots, mainly by restricting defence responses to specific root zones and cell layers (Chuberre et al., 2018). The PTI in roots also comprises the ROS (reactive oxygen species) production, sporadic and patchy callose deposition and growth rate modifications upon PAMP stimulation (Badri et al., 2008; Chuberre et al., 2018; Millet et al., 2010; Rich-Griffin et al., 2020; Zhang et al., 2022). Upon injury of RH, callose can be deposited locally in the RH cell wall as well, however, the identity of the callose synthase involved remains unknown (Galway et al., 2011). It has been recently shown that the defence-related callose synthase PMR4 is responsible for the RH callose deposition

upon phosphate starvation (Okada et al., 2023). The RH can react to pathogenic bacteria (e. g. *Pseudomonas syringae*), similarly to the beneficial ones, by the enhancement of the RH growth (Pečenková et al., 2017; Zamioudis et al., 2013). Unlike living bacteria, elicitor treatments in Arabidopsis do not provoke prominent RH growth changes, except for the DAMP PEP1 (Okada et al., 2021).

Both RH tip growth and pathogen sensing are under the control of development- and defence-related receptor kinases, and binding of their cognate ligands can for instance lead to the ROS production and/or activation of Ca2+ channels, such as CYCLIC NUCLEOTIDE GATED CHANNELS (CNGCs) (Ladwig et al., 2015)). The CNGCs produce transients with specific patterns, further transmitted to transcriptional reprogramming of defence (or symbiosis) (Yuan et al., 2017). Recent studies have reported that CNGC6, CNGC9 and CNGC14 are crucial for RH tip polar growth (Brost et al., 2019; Ladwig et al., 2015). A phosphorylation activation of mitogen-activated protein kinases (MAPK) cascade is another convergence point of signalling pathways. The MAPK3/6 signalling cascade plays a role in the RH growth (Rentel et al., 2004), as well as in plant immunity (including chitin-activated defence), together with the second MAPK4-comprising cascade (rev. in (Zhang and Zhang, 2022)).

The simplest way to study defence responses is by applying a single PAMP or immunity elicitor such as chitin or its derivate chitosan. Chitin is an insoluble polymer of β-1,4-linked N-acetylglucosamine, which is in Arabidopsis recognized by a complex of receptor and co-receptors - Chitin Elicitor Receptor Kinase 1 (CERK1) and lysin motif receptor kinases 4 and 5 (LYK4 and 5) (Cao et al., 2014; Miya et al., 2007; Wan et al., 2012). The chitin recognition activates the production of chitinases by plants; to avoid this recognition and hydrolysis by chitinases, fungi secrete chitin de-N-acetylases to convert chitin to chitosan. Fully deacetylated polymer units can still activate Ca^{2+} signalling-related subset of cellular responses, which in case of overactivation provokes cell death independent of the CERK1/ROS/MAPK pathway (Ye et al., 2020).

Chitosan is typically obtained from marine crustaceans´ chitin by chemical deacetylation (up to 90%) with molecular weights (Mw) ranging from oligo- (<5 kDa) to polysaccharides (70–100 kDa). Due to the protonation of glucosamine, chitosan molecules carry an overall positive charge. Chitosan functions as a PAMP (Iriti et al., 2006), but also as an antimicrobial factor causing intracellular ROS burst with subsequent oxidation of pathogen cell membrane fatty acids and plasma membrane

104 permeabilization (Lopez-Moya et al., 2017). Interestingly, high doses of chitosan in the
105 rhizosphere of Arabidopsis, tomato or barley significantly arrest root development,
106 probably via interference with auxin and gibberellic acid regulation or via activation
107 of jasmonic (JA) and salicylic acid (SA) related genes in roots (Lopez-Moya et al., 2017;
108 Suwanchaikasem et al., 2022).

109 In this report, we compare the elicitation of plant immunity with two different
110 chitosan concentrations, low 0.001%, further referred to as LCC, and high, 0.01%
111 further referred to as HCC, focusing on RH reactions. We bring evidence of the plant
112 capability to adjust the RH rate growth, as well as to reinforce the RH cell wall by the
113 callose deposition. The observed RH-specific effects are dependent on the chitosan
114 concentration, but not its molecular size, and are present also in the functionally
115 analogous but evolutionary non-related structures, namely rhizoids of the liverwort
116 *Marchantia polymorpha* and rhizophores of the lycophyte *Selaginella uncinata*, as well as
117 in the regenerating protoplasts of *Physcomitrium patens*. Further, on the subcellular
118 level, we tested the responsiveness of RH endomembranes and cytoskeleton to
119 chitosan treatments. To understand the impact of the chitosan treatments on overall
120 plant growth and defence, we performed Ca^{2+} and MAPK signalling assays and
121 RNAseq analysis, pointing to limited but significant changes caused by LCC,
122 compared to HCC treatment. Out of these experiments, we could conclude that the RH
123 callose deposition is the consequence of the mild biotic stress affecting the cells with
124 the intensive growth rate, while the stronger biotic stress provokes almost immediate
125 and more prominent tip-localised endomembrane changes and RH growth cessation.
126 Our results thus reveal the unexpected aspects of the RH growth-defence trade-off,
127 and set the basis for possible future modifications of the plant fitness using mild and
128 environmentally low-impact treatments.

129 **Results**

130 **Chitosan treatment induces concentration-dependent root growth changes and**
131 **callose deposition also in root hairs**

132 When the 5-7 day-old *A. thaliana* seedlings in liquid medium were treated with
133 several different concentrations of chitosan 0.0001% - 0.01%, 24 h post treatment we
134 could observe the ectopic callose deposition in cotyledon leaves, but also in roots and
135 RHs (Figure 1A). While the LCC (0.001%) induced small callose deposits in leaves, no
136 primary root growth inhibition and prominent callose depositions in RH regions close
137 to the root tips, the HCC (0.01%) induced larger callose deposits in leaves, prominent
138 primary root growth inhibition and no callose in root hairs. Conversely, plants

139 incubated with very low chitosan concentration (0.0001%) were indistinguishable from
140 the mock treatment by both the lack of prominent callose deposition and no inhibition
141 of the primary root growth (Figure 1A, B). Given the striking response of RH to specific
142 chitosan concentration (LCC, 0.001%), we wondered if it is caused by the particular
143 chitosan composition. We therefore tested the effect of the same low concentration for
144 several other chitosan variants with different Mw, viscosity, and solubility. The
145 observed effect on the callose deposition along RH was consistent for all analysed
146 chitosan variants but not for the non-deacetylated chitin, confirming that the RH
147 callose deposition is chitosan-specific (Figure 2). When the seedlings were treated by
148 LCC in distilled water, which does not support the RH growth such as liquid ½ MS,
149 there was no callose deposition in existing RHs, pointing to the fact that the callose is
150 deposited only in newly growing RH exposed to chitosan (Supplementary figure 1A).
151 Similarly, the application of HCC provokes strong RH growth inhibition without
152 observable RH callose deposition (Figure 1, Supplementary figure 1B).

153 We could conclude that chitosan provokes specific responses in both above-
154 ground organs and root hairs, depending on the applied concentrations.

155 **Callose deposition is PMR4-dependent and uncoupled from the RH growth**
156 **inhibition**

157 In order to uncover the key players in the RH callose deposition, we decided to
158 analyse the RH modifications in the *gsl5/pmr4* mutant lacking the callose synthase
159 isoform responsible for the pathogen-induced callose deposition. The LCC-induced
160 callose deposition was completely abolished in the *pmr4* mutant (Figure 3A). Further
161 on, when using the GFP-tagged PMR4 construct (Sabol et al., in preparation), we could
162 observe a higher accumulation of PMR4 on the tip of the newly growing RH 4h after
163 the chitosan addition in comparison to the mock treatment (Figure 3B). Along with the
164 callose *pmr4* mutant, we tested *cals8-1,* which is involved in the biotic stress-related
165 regulation of plasmodesmatal permeability, as well as a range of secretory, defence-
166 related (including signalling co-receptor *bak1* and chitin receptor *cerk1*) and
167 phytohormone mutants, however, for all of them we found the RH callose pattern
168 similar to the one in WT/Col-0 (Supplementary figure 1C).

169 Since the LCC caused a decrease in RH growth, we hypothesised that it may be
170 coupled with callose deposition and rigidification of the RH cell wall. However, the
171 LCC-induced RH growth decline in the *pmr4* mutant that does not deposit callose was
172 similar to that of WT/Col-0 (Figure 3A). We also monitored both callose deposition and
173 root hair growth in WT after the LCC addition, showing that the callose starts to

174 accumulate already at 4h time point, while the average inhibition of the root hair
175 growth starts to be evident after 8h, reaching significant difference from mock
176 treatment approximately 12 h after addition of chitosan (Figure 3C and 3D). This
177 difference in the time course pattern further confirms the independence of the RH
178 growth decline and callose deposition. In contrast to LCC, the HCC treatment
179 completely arrested the growth of new RHs already at the 4h time point
180 (Supplementary figure 1B).

181 The LCC-induced callose deposition in RHs is thus PMR4-dependent and
182 uncoupled from the mechanisms underlying slower RH growth.

183 **Low concentration chitosan treatment triggers weak PTI-related signalling**

184 We further wanted to uncover differences in general activation of PTI responses
185 between the LCC and HCC treatments. For that purpose, we first followed calcium
186 spiking using sensor R-GECO1 construct (Keinath et al., 2015) in a 20 min treatment of
187 seedlings by the two concentrations of chitosan. There was only a mild Ca^{2+} increase
188 in spiking in LCC treatment compared to HCC treatment, which triggered more
189 prominent peaks of intracellular Ca^{2+} increase (Figure 4A). Besides their intensity, the
190 two treatments also differ in their patterns and peaking time, evidencing early
191 specificity of the LCC versus HCC. Interestingly, despite the obvious employment of
192 the Ca^{2+} channels in chitosan sensing, *cngc* mutants have unaffected deposition of the
193 callose to the RH cell walls, indicative of higher importance of the CNGC-mediated
194 signalling for the RH growth than for the callose deposition (Supplementary figure
195 1C).

196 Additionally, we assayed another parallel early signalling PTI pathway, MAPK
197 activation, after the two chitosan concentrations 30 min long treatments. Similarly, a
198 western blot analysis of MAPK activation by phosphorylation (quantified as a ratio of
199 band intensities obtained for the phosphorylated part and whole pool MAPKs)
200 demonstrates significant MAPK activation in both cases. However, HCC causes a more
201 prominent effect on the MAPK signalling pathway than the LCC (Figure 4B and C).
202 The distribution of activation along the three tested MAPKs - MAPK3,6 and 4 was
203 similar for both treatments.

204 Accordingly with these results, the pretreatment of seedlings with HCC, and
205 not LCC, causes significant enhancement of PTI, as demonstrated by the bacteria
206 sensitivity and amplification assay upon seedlings inoculation with *Pseudomonas*
207 *syringae pv. tomato* mutant in T3 secretion system *hrcC* (Pst *hrcC*; Figure 4D).

208 These results confirm that the LCC treatment, similarly to the HCC one,
209 activates PTI-related signalisation, nevertheless, the pattern and intensities of these
210 activations significantly differ.

211 **Chitosan modulates rapid calcium and endomembrane dynamics but not**
212 **actin cytoskeleton in growing root hairs**

213 Having shown distinct fast calcium responses after LCC and HCC treatment,
214 we next analysed the spatiotemporal details of the Ca^{2+} reporter R-GECO1 within the
215 RH cells. In mock treatment, the very tips of RH undergo constitutive pulsatile changes
216 of R-GECO1 signal intensity, while the atrichoblasts´ R-GECO1 pattern transiently
217 changes upon the buffer exchange during the mock treatment, and much more
218 prominently upon chitosan treatments (Figure 5A and B, Supplementary video). Each
219 of the applied treatments causes specific RH Ca^{2+} influx intensities and patterns, with
220 LCC treatment causing even a decrease in the RH-tip located cytoplasmic Ca^{2+} during
221 the initial phase of the treatment (Figure 5C). Interestingly, upon HCC, a wave of R-
222 GECO1 signal often starting within 1-2 min at the RH tips and moving to the RH cell
223 interior and further on through trichoblast toward other root cells was observed
224 (Supplementary video).

225 We then tested if and how the chitosan-triggered early signalling event affects
226 the intracellular dynamics. We focused on well-growing RH close to the root tip, and
227 after applying mock, LCC and HCC treatments, we followed intracellular changes in
228 localisation and dynamics of vacuolar and cytoskeletal genetic markers, as well as
229 endocytic dye FM4-64 in a real-time approach (Figure 6). We monitored treated RH
230 for 0-30 minutes. First, we could observe an immediate and significant root hair
231 growth cessation in the case of HCC-treated seedlings, often accompanied by RH
232 damaging and bursting. In addition, for LCC we could also observe significantly lower
233 average growth rates. Nevertheless, out of the obtained data distribution, we could
234 conclude that in the case of this treatment, RHs mostly either prominently slow down
235 their growth, or they grow at rates similar to mock-treated root hairs (Figure 6A).
236 Interestingly, the vacuolar dynamics does not follow the trend found for growth and
237 the RHs react to the two treatments contradictory – while LCC causes small and
238 insignificant enhancement in vacuolar dynamics, HCC impairs the vacuolar dynamics
239 in the RH tip area (Figure 6B). The cessation of vacuolar movement in the RH tip upon
240 HCC treatment may be related to observation obtained for the same treatment on the
241 enhanced FM4-64 dye accumulation in RH endocytotic/vesicular compartment,
242 probably as a consequence of collapsing endomembrane trafficking (Figure 6C).

243 Since vacuolar dynamics is often governed by the actin cytoskeleton, we tested
244 the effect of various chitosan concentrations on the organization and dynamics of
245 filamentous actin in RHs. Somewhat unexpectedly, there was no difference in the actin
246 organisation during the early response to chitosan, as dynamics of actin-decorating
247 fimbrin-GFP were indistinguishable among the mock, LCC, and HCC treated plants
248 (Supplementary figure 2).

249 The microscopical observations thus confirmed that the LCC, despite
250 provoking prominent changes in CW composition and RH growth inhibition in later
251 time points, does not impose a prominent stress that would disturb endomembrane
252 compartments in early time points. On the other hand, HCC treatment significantly
253 inhibits RH growth, rapidly affects calcium gradient and oscillations in RH tip, blocks
254 vacuolar dynamics and provokes accumulation of endocytotic/FM4-64 marked
255 compartment.

256 **Chitosan induces changes in gene expression and cell wall components**

257 To obtain a more general view on chitosan responses and to gain another insight
258 into distinct plant reactions to LCC and HCC treatment, we performed the RNAseq
259 analysis of liquid medium-grown Arabidopsis seedlings treated with mock, LCC or
260 HCC for 24 h. The general responsiveness of plants to LCC is far less dramatic than
261 what is observed on the level of RHs, as only 58 differentially expressed genes (DEGs)
262 were identified for LCC, and 8507 for HCC, comprising participants of plant PTI
263 responses; most of the DEGs found for LCC are also present in the HCC DEG gene set,
264 while only 11 genes are specifically regulated by LCC (Table I; Supplementary table I).
265 Out of these 11 DEGs, 10 genes are downregulated, and only one, AtLRX6 (Leucine-
266 rich repeat-extensin 6; AT3G22800), upregulated and found to belong to leucine-rich
267 repeat/extension-type proteins, reported previously to play a role in RH growth. We
268 have also identified genes which were differentially expressed in LCC and HCC
269 treatments - in contrast to HCC which upregulates their expression, LCC
270 downregulates (bottom 5 genes in the Table I). The restricted number of DEGs
271 provoked by LCC is in concordance with milder Ca^{2+} and MAPK responses activation
272 and with limited morphological changes observed mainly on the level of newly
273 growing RHs, implying that the RH callose encasement is an effective but limited and
274 localised strategy for the plant to overcome mild biotic threats, and to proceed with
275 undisturbed development.

276 Even though our results are centred around seedlings' roots reactivity to
277 chitosan, in order to obtain a more general view of the LCC impact on plants, we

278 analysed LCC-caused gene expression of adult rosettes, and we encountered the
279 results with those from the cell wall profiling of the LCC-treated rosette leaves
280 (Supplemental figure 3A, 3B; (Voxeur et al., 2019)). Interestingly, the RNAseq of LCC-
281 treated mature rosette leaves revealed differences that are more prominent and more
282 similar to expression patterns provoked by other elicitor treatments, and mainly more
283 similar to the HCC-treated seedlings. Both RNAseq and cell wall composition analyses
284 accordingly revealed the affection of pectin synthesis and modification/methylation
285 states upon LCC. We next realised an enzymatic fingerprinting of the
286 homogalacturonans and xyloglucans using a commercial polygalacturonase and an
287 endo-cellulase, respectively, from 5-weeks-old Arabidopsis leaves treated in presence
288 of mock and LCC. We analysed the oligosaccharide produced by LC-MS (Paterlini et
289 al., 2022). It revealed that LCC treatment likely triggered the demethylesterification
290 and acetylesterification since the relative amounts of GalA4Me decreased and GalA3
291 Ac increased, respectively. Chitosan treatment also modified the structure and
292 composition of hemicellulose building blocks. It remains to be further assessed
293 whether, and how the CW components modifications take part in the RH
294 responsiveness to chitosan.

295 **Callose deposition is conserved in evolutionarily unrelated structures functionally**
296 **analogous to root hairs**

297 Because the callose deposition was preserved in all tested signalling and/or
298 secretory pathway mutants, we speculated that it is a robust reaction which might be
299 evolutionary conserved and present also in non-angiosperm plant lineages and their
300 stress responses. In a similar experimental setup with plants cultivated in the liquid
301 medium, we were able to induce the growth of the morphological structures
302 functionally analogous to root hairs, namely rhizoids in the liverwort *Marchantia*
303 *polymorpha* and the rhizophores of spikemoss *Selaginella uncinata*. When the plants
304 were treated for 24 h with LCC, *M. polymorpha* rhizoids growing out of an asexual
305 reproductive body gemma were enclosed by callose, similarly to rhizophore surface
306 cells of *S. uncinata* (Figure 7). Also, no callose depositions were detected in mock, while
307 HCC treatment prevented their appearance, mirroring the situation with RH of *A.*
308 *thaliana*.

309 We further verified if the relation of chitosan treatment and callose response can
310 also be established for different unicellular model – regenerating protoplasts derived
311 from the moss *P. patens* tip growing protonemal cells (Brejšková et al., 2021; Cove et
312 al., 2009). We could indeed observe a prominent callose deposition caused by LCC,

313 while HCC treatment had a deleterious effect on protoplast viability and regeneration
314 (Supplementary figure 4A). Interestingly, in contrast to *P. patens* regenerating
315 protoplasts, above-ground tissue-derived protoplasts of *A. thaliana* did not deposit
316 callose while regenerating in the presence of chitosan (Supplementary figure 4B).

317 These results confirmed that the potential of RH and RH-like structure to
318 deposit callose is an evolutionary old intrinsic feature. This capacity, however, may be
319 exclusive for the tissue derived from the non-aerial plant parts, exhibiting fast cellular
320 growth and newly generating the cell wall.

321 **Discussion**

322 In this work, we uncovered the RHs capability to perceive the chitosan as an
323 elicitor, and depending on its concentration, to deposit callose to the cell wall and/or
324 to inhibit RH growth. The two processes are not mutually dependent, and the two
325 studied chitosan concentrations, the low (LCC) and the high ones (HCC), may induce
326 plant responses that overlap in their quality and quantity, but also those which are
327 specific. We also demonstrate that the shift in treatment stringency toward the milder
328 concentrations of the stressor can reveal new defence- and development-related
329 phenotypes.
330 Phytopathological studies often deal with approaches involving high elicitor
331 concentrations necessary to provoke responses that could be easily observed and
332 quantified (Aslam et al., 2009; Luna et al., 2011). We speculate that the low chitosan
333 concentration (LCC, 0.001%), used in our study, imposes a mild biotic stress, which
334 young plants can sustain, and to which they react by the adjustments on the level of
335 RHs (as the most exposed cell type) by slowing down their growth rate and by
336 fortifying the cell wall with callose. Besides RHs, the LCC stimuli are also perceived
337 by other root parts and also above-ground organs, as our results from Ca^{2+} and MAPK
338 assays showed. Interestingly, prolonged LCC treatment had no impact on the growth
339 of young plants, and they are not affected in their further development, implying an
340 accommodation to these low chitosan concentrations, also observable in quenching of
341 early phases of Ca^{2+} spiking patterns. In agreement with early signalling patterns, and
342 results of the RNAseq and CW analysis, the susceptibility assays showed an
343 enhancement of resistance of plants to Pst *hrcC* bacteria when applied upon HCC
344 pretreatment, while the effects of LCC leaves no durable effect on the immunity of
345 young seedlings.
346 Similarly, the RNAseq data from LCC- and HCC-treated seedlings corroborate
347 the existence of primarily quantitative differences between the two treatments since

348 only a minority of DEGs was found to be specific for LCC. Despite the scarcity of the
349 LCC-specific candidates, we consider that the role of one of the identified DEGs,
350 LRX10, is worthy of further verification, since this protein, together with related pollen
351 tube-expressed isoforms, has been found to be involved in the pollen tube cell wall
352 pectins and callose deposition, important for the process of fertilisation (Wang et al.,
353 2018) Therefore, the presence of minor qualitative differences is legible as well. This is
354 further fortified by the fact that, unlike the HCC treatment, which impairs plant
355 growth by affecting the auxin pathway (Lopez-Moya et al., 2017), the LCC has only a
356 minor effect on auxin signalling enhancement, as demonstrated using the DR5::GFP
357 auxin reporter line (Supplemental figure 5).

358 Callose deposition is typically described as an early defence response in leaf
359 tissue, where it serves mainly to seal the plasmodesmatal connection between cells to
360 prevent pathogen spread and nutrient withdrawal (Epel, 2009) or to prevent
361 pathogens' entrance (Meyer et al., 2009; Ortmannová et al., 2022)), but also in primary
362 root epidermis after the defence-eliciting treatments, displaying a similar spotty
363 pattern as found in leaves (Millet et al., 2010). In agreement with this defence
364 involvement, callose deposition is repressed in the establishment of mutualistic
365 interactions (rev. (German et al., 2023)). Besides the defence-related functions, callose
366 also serves as a mechanical support in the new cell wall formation, in the pollen exine
367 formation and germinating-pollen plug, but also in a functional specialisation of
368 trichome basal parts (Kubátová et al., 2019; Kulich et al., 2015; Ma et al., 2021;
369 Motomura et al., 2022). The RH callose deposition observed by us is tightly coupled
370 with a state of the elongating root cells, and in the newly growing root hairs in the
371 zones closest to the root tip. Therefore, we hypothesise that the RH callose coating is
372 the consequence of two processes going along – of the elicitor caused defence
373 signalling, as evidenced by the dependance on the typically pathogen-induced isoform
374 of callose synthase PMR4, but also of the fragile and immature state of the cell wall
375 undergoing synthesis, which was additionally confirmed on our experiments with
376 regenerating protoplasts that readily deposit callose upon the LCC treatment (Dehors
377 et al., 2019), as well on recently demonstrated abiotic stress and starvation related RH
378 callose deposition (Okada et al., 2023).

379 Both LCC / HCC treated rhizoids/rhizophores of *M. polymorpha* and *S. uncinata*,
380 despite their evolutionary unrelated origins, provide the same morphological and
381 subcellular responses, including the employment of the evolutionarily conserved
382 callose synthases. This functional conservation in terrestrial plants might have an
383 origin in the callose contribution to the newly formed post-meiotic cell wall of spores
384 or pollen. Secondarily, these independently-evolved mechanisms may have also been

involved in the onset of responses of plant cells to the hostile environmental conditions of land/soil, also including pathogen threat (Herburger and Holzinger, 2015; Ks et al., 2020).

Unlike LCC, the HCC has a prominent effect on the appearance and subsequent loss of complexity of the RH tip-localised portion of the vacuolar compartment. The HCC causes the vacuolar withdrawal and dismission of the complex tubular tip-localised vacuolar growing parts. Given the massive uptake of FM4-64 dye in HCC-treated RHs, this may be the consequence of the enlargement of the endocytic zone in the RH tip, or an unrelated endomembrane response. The prompt response of vacuolar dynamics to chitosan may suggest that, besides a proposed role for vacuolar calcium channels in mechanosensing of the tip-growing cells, a part of the pathogen sensing might reside on the tonoplast as well (Radin et al., 2021).

Despite the critical importance of the actin cytoskeleton in both RH growth and responsiveness to pathogens, in our experiment, at an early time points, there was no significant modification of fimbrin-GFP-labelled actin filaments upon chitosan treatments (Supplementary figure 2, see also (Porter and Day, 2016; Ringli et al., 2002; Sun et al., 2021; Vaškebová et al., 2018)). It would be interesting to verify if this observation might be related to the different requirements for the callose- and cellulose synthases localization along the plasma membrane by the microtubules and the actin, respectively, similarly to what has been found for the tobacco pollen tube (Cai et al., 2011).

In addition to demonstrating the usefulness of mild chemical/eliciting treatments of plants for opening new perspectives in plant studies, we are also suggesting the simple experimental setup based on a single, exposed, and sensitive cell. This approach could be further employed for gaining the knowledge on the root and RH-related immunity, as well as in the studies of the overall plant fitness in relation to the rhizosphere conditions.

Conclusions

The effect of the low concentration chitosan treatment on Arabidopsis root hairs, and similar effect in Marchantia and Selaginella rhizoids or rhizophores, expose their unexpected deeply rooted capacity to react by the callose accumulation in response to this fungal elicitor. The root hair cell wall callose deposition is PMR4/GSL5-dependent and occurs in parallel but independently of the root hair growth inhibition. The higher chitosan concentration treatments cause prominent root hair growth inhibition that precludes the callose deposition, leading to the phenotypic difference between the two treatments. The intensive root hair growth inhibition is

421 probably the consequence of the emphatic defence alerting, as well as interference with
422 the root tip-localised vacuolar and endocytic compartments.

423 **Material and methods**

424 **Plant cultivation**

425 For seedlings and plants cultivation, seeds were surface sterilised (5 min in 70%
426 ethanol, 2 × 5 min in 10% commercial bleach, rinsed three times in sterile distilled
427 water) and stratified for 2–3 days at 4°C. Seeds were then germinated and grown on
428 vertical ½ MS agar plates (half-strength Murashige and Skoog salts, Duchefa
429 Biochemie, supplemented with 1% sucrose, vitamin mixture, and 1.6% plant agar,
430 Duchefa Biochemie) at 21 °C and 16 h of light per day for five-seven days. For
431 propagation of plants, seedlings were transferred into Jiffy Products International
432 pellets and grown at 22 °C and 16 h of light per day in growth rooms.

433 The following previously published Arabidopsis mutant and transgenic lines
434 were used in this study: *aux1-21* (CS9584, (Bennett et al., 1996)), *bak1-4* (CS71777;
435 (Kemmerling et al., 2007)), *cals8-1* (SALK_037603; (Cui and Lee, 2016)), *cerk1-1*
436 (pst14772; (Miya et al., 2007)), *cngc14-1* (SALK206460; (Shih et al., 2015)), *cngc2-3*
437 (SALK_066908; Chin et al., 2013), *exo70H4-1* (SALK_023593; (Kulich et al., 2015)), *npr1*
438 (CS3726; (Cao et al., 1994)), *pmr4-1* (CS67159; (Vogel and Somerville, 2000)), *rbohD-3*
439 (N9555, Torres et al., 2002 11756663), UQ10::GFP-PMR4 (Kulich et al., 2018),
440 promPMR4::GFP-PMR4 (Sabol et al, in preparation), DR5-GFP (Heisler et al., 2005),
441 fimbrin-GFP (Wang et al., 2004), and vacuolar ATPase Vti-GFP (gifted by Karen
442 Schumacher, Heidelberg). The wild type (WT) Col-0 was used as control. When
443 needed, primers used for the genotyping were the same as used in the above-cited
444 original studies.

445 **Chitosan treatment**

446 Plants were propagated in vitro for 5-7 d on vertical plates, and then transferred
447 by forceps into liquid ½ MS (control) or liquid ½ MS with chitosan added (100x and
448 1000x diluted stock solution of the 1% chitosan in 1% acetic acid), usually 4-8 plants
449 per 3 ml, in 6-multiwell plates (Nunclon, Thermo Fisher Scientific). Plants were
450 cultivated for 24 h 16/8 h light/dark at 21–22°C without shaking. After 24 h of
451 incubation, plants were transferred to 3 ml of ethanol for 6-24 h at room temperature
452 for destaining, with mild shaking, and subsequently transferred into 3 ml of 150 mM
453 K2HPO4. After 1 h, aniline blue (final concentration 0.005% solution in 150 mM
454 K2HPO4) was added and seedlings stained for additional 24 h with mild shaking and
455 observed under the microscope. Additional verifications confirmed that there were no
456 differences between the mock treatment with and without corresponding dilution of

457 acetic acid. Several chitosans used for analyses were purchased from Merck, Germany
458 (Cat. Nos C3646, 523682, 448877 and 419419), as well as chitin (C7170).

459 **Root and root hair phenotype examination**

460 The plant responses to pathogens were monitored by microscopy and
461 documented by photography. The seedlings were placed on microscopic glass, their
462 primary root stretched and lengths measured. Microscopic analysis of root tips and
463 root hairs was performed using an Olympus BX51 microscope with attached DP50
464 camera (Olympus). For each treatment/genotype 5-10 plants were photographed and
465 analysed. Root hair lengths were determined for the first 20-40 root hairs starting from
466 the root tip for each plant; for statistical analysis. Callose deposition was analysed
467 using the pre-set conditions for bright-field and DAPI, and objective 5x or 10x.

468 **Protoplasts preparation**

469 The moss *Physcomitrium patens* Gransden strain was routinely propagated in
470 vitro on BCD medium supplemented with ammonium tartrate dibasic (BCDAT),
471 according to (Cove et al., 2009), in a climate chamber (16 h of light/8 h of dark, 25 °C,
472 illuminated by fluorescent tubes at 50-70 μmol m^{-2} sec^{-1}). Protonemal tissue (6-7 days
473 after propagation) from cellophane-grown culture was transferred into the
474 1%Driselase/8%mannitol solution. When filamentous structure became invisible
475 (approx. 1 h at RT), protoplast suspension was filtered via/through 100 μm steel mesh.
476 Protoplasts were diluted in 8% mannitol up to 10 ml and spun down (700 rpm for 4
477 min, without brake) and this step was repeated three times. Protoplast sediment was
478 carefully resuspended between centrifugations to avoid aggregation of protoplasts.
479 Finally protoplasts were incubated in the liquid regeneration medium (BCDAT+ 5mM
480 NH_4+ 6% w/v mannitol + 10 mM $CaCl_2$) overnight at RT. Arabidopsis protoplasts were
481 prepared according to (Yoo et al., 2007). Briefly, Arabidopsis leaves from 3-4 weeks old
482 plants grown under short day conditions (8/16 h light/dark) were cut onto 2 mm
483 stripes. The 2 g of prepared plant tissue were submerged in 37 °C warm protoplast
484 solution (0.4M mannitol, 1.5% cellulase, 0.4% macerozyme, 20mM MES pH 5.7, 20mM
485 KCl, 0.1% BSA, 10mM CaCl2) and vacuum has been applied for 30 min. The
486 submerged leaves were kept in the dark in RT. After 3 h, the flasks with protoplasts
487 were gently swirled and the quality of protoplasts was checked with a microscope.
488 The protoplast solution was washed with a WI buffer (4mM MES pH 5.7, 0.5M
489 mannitol, 20mM KCl), filtered through miracloth and clarified with multiple
490 centrifugations (3x100g, 2 min). For the recovery of protoplasts, 0.7 ml of WI solution
491 in a 12-well plate was applied. Both types of protoplasts were left to recover for 3h,
492 and were subsequently treated with chitosan or mock for 24 h. Protoplasts were

493 stained with aniline blue and the final condition of protoplasts monitored with the
494 microscope Olympus BX51 microscope with attached DP50 camera.

495 **Selaginella and Marchantia propagation and callose deposition assay**

496 For sterile *Selaginella uncinata* ('Comenius' strain) culture establishment, excised
497 fragments containing meristems were washed with distilled H_2O and surface sterilized
498 with 70% EtOH (1 minute) and subsequently with 40% commercial bleach (SAVO)/2%
499 sodium hypochlorite for 15 minutes and rinsed with a sterile water twice (Park et al.,
500 2020) . Axenic regenerants were subsequently vegetatively propagated on ½ MS media
501 with 0.6% agar under standard conditions (22°C, 16/8 light/dark, ca. 180 μmol/m^2/s).
502 Chitosan treatments were performed on whole regenerating plantlets interchangeably
503 with the *Arabidopsis thaliana* approach.

504 *Marchantia polymorpha* Tak-1 has been maintained on ½ Gamborg media
505 ((Gamborg et al., 1968); G0210 Duchefa) supplemented with 1,2% agar under standard
506 conditions (22°C, 16/8 light/dark, ca. 180 μmol/m^2/s). Chitosan treatments were done
507 with gemmae analogously to an *Arabidopsis thaliana* procedure, with a slight change,
508 where the liquid ½ MS has been replaced with ½ Gamborg media supplemented with
509 1% sucrose to enhance the rhizoids initiation**.**

510 **Confocal and Real Time microscopy**

511 Small agar block with *in vitro* cultivated 6-day-old seedlings was gently cut
512 from the cultivation plate and transferred into sterile microscopic chambers containing
513 100 ul of liquid ½ MS. Chambers were covered with lids and left overnight in a
514 cultivation chamber. For real time treatments we used custom designed 3D printed
515 perfusion add-on which fits into the microscopic chamber and allows exchange of
516 media inside the microscopic chamber during microscopy session. To mediate the
517 exchange we used medical grade silicone tubes mounted onto a peristaltic pump and
518 perfusion add-on with speed approximately 100 ul/min. All microscopic samples were
519 10 min pretreated with the mock solution right before capturing, chitosan treatment
520 was applied directly during the microscopic session. For mock treatments the liquid
521 1⁄2 MS was used. For chitosan treatments, 0.001% chitosan (LCC) or 0.01% chitosan for
522 HCC were added into the ½ MS. For the FM4-64 (Thermofisher scientific) staining we
523 used the same perfusion settings and solutions just with the addition of 0.001% FM4-
524 64 dye (1 mM stock solution). Samples were treated for 15 min before observation.

525 For RH R-GECO1 signal intensity analyses the same microscopic perfusion add-
526 on was used. The 5-6 day old RGECO1 expressing seedlings were transferred into
527 microscopic chambers, covered with a lid and kept overnight in the cultivation room.
528 Samples were treated using the same chitosan solutions as in previous experiments
529 (LCC, HCC). Roots were captured every 1 second for 7 min for each part (untreated,

530 mock, LCC, HCC) in the case of LCC and HCC we added 30 seconds long (capturing
531 time one frame per 0,1 second) to monitor fast changes. These super-fast scanning parts
532 were removed for the figures.

533 Real Time imaging was done on the Spinning disc (SD) microscope Nikon
534 (Eclipse Ti-E, inverted) with Yokogawa CSU-W1 SD unit (50mm) equipped with
535 Omicron LightHUB ULTRA light source, Plan-Apochromat L 20x/0.75 or Plan-
536 Apochromat LS 40x/1.25 WI objectives were used for capturing. Microscope is
537 operated by NIS Elements 5.30 software. GFP was observed using a 488 nm excitation
538 laser with Semrock brightline Em 525/30 filter. FM4-64 was observed using a 488 nm
539 excitation laser with Semrock brightline Em 641/75 filter.

540 **F**or the analysis of vacuolar dynamics a *stack difference* task inside *mutli*
541 *kymograph* plugin ImageJ (FIJI) followed by analysis of *moments* thresholded area of the
542 result image was used. See Supplementary material *VD_macro.ijm.*

543 For the FM4-64 uptake analysis the average Z projections of single RH were
544 taken with subsequent analysis of signal intensity within inner cell space (ImageJ -
545 FIJI). Actin dynamics wes analysed using the same procedure but with longer gap
546 between consecutive frames (10 seconds).

547 **Ca2+ signalling reporter imaging and evaluation**

548 *A. thaliana* seedlings expressing R-GECO1 Ca2+ signalling reporter were
549 vertically grown in a growth chamber at 23 °C by day (16 h), 18 °C by night (8 h), 60%
550 humidity and light intensity of 100 μmol photons m^{-2} s^{-1} (Keinath et al., 2015).
551 Microfluidics experiments were performed using four-day-old seedlings placed into a
552 microfluidic chip and enclosed by a cover glass (Serre et al., 2021). Channel one
553 contained a control solution (½ MS, fluorescein dextran 6 μg/ml), while channel two
554 contained a treatment solution (½ MS, 0.01% or 0.001% chitosan). The media flow rate
555 was 3 μl/min (OBI1, MFS2 Elveflow, and Elveflow software ESI (v.3.04.1). The system
556 was mounted to a vertical microscope stage and kept for 15 min plant recovery. The
557 media exchange was indicated by fluorescein-dextran signal intensity.

558 Plants were imaged using a vertical stage Zeiss Axio Observer 7 with a
559 Yokogawa CSU-W1-T2 spinning disk unit with 50-μm pinholes equipped with a VS-
560 HOM1000 excitation light homogenizer (Visitron Systems), objective Zeiss Plan-
561 Apochromat ×10/0.45. Images were acquired using VisiView software (Visitron
562 Systems, v.4.4.0.14). R-GECO1 was excited by a 561 nm laser, and fluorescein dextran
563 by a 488 nm laser. The signal was detected using a PRIME-95B Back-Illuminated
564 sCMOS camera (1,200 × 1,200 pixels; Photometrics). The seedlings were imaged every
565 13 s for 60 min. The signal intensity of R-GECO1 was measured inside the root at the
566 root late elongation zone using ImageJ Fiji software (Schindelin et al., 2012). The

567 intensity of the background was measured in areas not affected by the root response
568 and subtracted from the R-GECO1 values. The intensity of fluorescein-dextran was
569 measured outside of the root. The data were normalised using division by initial
570 fluorescence intensity values (F/F0). As the initial value F0, we used the average
571 fluorescence intensity at five-time points before treatment.

572 **RNA isolation and RNAseq analysis**

573 RNA was isolated from young, 6-7-day-old whole seedlings (transferred from
574 vertical ½ MS plates to liquid ½ MS for treatments), and adult (5-6 week old) rosette
575 leaves of *A. thaliana* plants, using the RNeasy Plant kit (Qiagen) according to the
576 manufacturer's instructions. Isolated RNAs were stabilised by GenTegra technology
577 microtubes (GenTegra, Pleasanton, California, USA). Strand-specific cDNA libraries
578 were constructed from polyA enriched RNA and sequenced on the Illumina
579 NovaSeq6000 platform with subsequent analysis performed by Eurofins. The RNA-
580 seq data used in this study are deposited in the National Center for Biotechnology
581 Information Gene Expression Omnibus database under the accession number
582 GSE239633.

583 **Protein extraction, western blot and MAPK assay**

584 Total protein extracts were isolated from 5–7-day-old *A. thaliana* seedlings
585 according to procedure described in (Fernandez and Beeckman, 2020). Briefly,
586 untreated and chitosan treated tissue samples were ground in liquid nitrogen and
587 dissolved in an extraction buffer containing Phosstop (Roche), and the concentration
588 of proteins determined by the Bio-Rad protein assay kit with bovine serum albumin
589 (BSA) as the standard. The extracts were denatured by boiling in a 6× SDS loading
590 buffer. The protein samples were separated by 10% SDS-PAGE and analysed by
591 Western blot using the α-p44/42-ERK antibody (SAB4301578), anti-MAPK3 (M8318,
592 Sigma), anti-MAPK4 (A6979, Sigma), and anti-MAPK6 (A7104, Sigma). The primary
593 antibodies were incubated with the membranes for 3 h at room temperature in the
594 blocking solution. Horseradish peroxidase-conjugated antibodies (anti-rabbit and
595 anti-mouse; Promega) were applied followed by chemiluminescent ECL detection
596 (Amersham) by the Bio-Rad documentation system. Using the Gel Analysis function
597 of ImageJ, signal intensities for protein bands were determined for each treatment
598 from 3 different samples. Loading consistency was examined by staining the
599 membrane with Ponceau S.

600 **Bacterial assay**

601 Bacteria susceptibility assay was performed according to Ishiga et al., 2011 and
602 Pečenková et al., 2020 with modifications. Briefly, plants grown in vitro (½ MS, at 21°C,
603 12 / 12 h of light / dark per day, for 6 days) were transferred to liquid ½ MS in 6-well

604 plates, and pretreated with mock, or with chitosan (LCC and HCC). After 24 h, the
605 medium was exchanged, and the *P. syringae pv. tomato hrcC* (Pst *hrcC*) OD = 0.01, was
606 used for seedlings inoculation. After the 24 h incubation with mild shaking 50
607 rpm/min, ten seedlings in one sample, always three samples for each treatment, in two
608 replications) were homogenised, homogenates subsequently diluted in series, plated
609 out, and after approximately 24-36 h of incubation on 28°C colonies counted.

610 **Cell wall preparation and enzymatic fingerprinting**

611 For cell wall analysis plants have been propagated in Jiffy pellets for 5-6 weeks,
612 10/14 h of light/dark regime. Plants were treated by dipping into the mock (distilled
613 water with 0.005% Silwett) or LCC chitosan (distilled water with 0.005% Silwett and
614 0.001% chitosan), and left for 24 h in the growth chamber. Treated and non-treated
615 samples were submerged in 96% (v/v) ethanol and boiled at 70°C for 10 min. The
616 pellets were collected by centrifugation (13000 g for 10 min) and dried in a speed
617 vacuum concentrator at 30°C overnight. Samples were digested with 1 U/mg DW
618 sample of *Aspergillus aculeatus* endo-polygalacturonase M2 (Megazyme, Bray, Ireland)
619 (Paterlini et al., 2022) in 50 mM ammonium acetate buffer (pH 5) at 37 °C for 18 h.
620 Samples were centrifuged at 13000 rpm for 10 min and 100 μL of the supernatants were
621 transferred into vials. The oligosaccharides released from digestion were analysed
622 according to (Paterlini et al., 2022).

623 **Image analysis and statistics**

624 Image processing software was employed for image data quantification. Roots
625 and root hair sizes were analysed using AnalySIS (Soft Imaging System GmbH,
626 Germany) or ImageJ (Schneider et al., 2012) software. The numerical data obtained
627 were processed using Microsoft Excel.

628 To determine statistical significance, Student's t-test and ANOVA tests were
629 conducted either using Excel or on-line calculators (http://in-silico.net, and
630 http://statpages.info/anova1sm.html). P-values of less than 0·05 indicated a significant
631 difference among the various groups. For multiple-comparison experiments, the
632 Kruskal - Wallis or Tukey Honestly Significant Difference (HSD) post hoc test were
633 used.

634

635 **Contribution**

636 M.D. performed root hair confocal microscopy, designed the experimental setup for
637 the real time observation of root hairs, performed microscopy and image analysis,
638 prepared RNA for RNAseq analysis, prepared figures and wrote the manuscript. S. H.
639 performed Selaginella and Marchantia experiments, and wrote the corresponding
640 parts in the manuscript. E. Š. performed MAP kinases assays. P. K. and M. F.

641 performed Ca2+-spiking recording and analysis. A. P. performed Pst *hrcC*
642 susceptibility assays. L. B. and J. O. prepared protoplasts and analysed their cell wall.
643 K. M. and N. S. analysed RNAseq data. A. V. and S. V. did the cell wall fingerprinting
644 analysis. G. C. verified callose deposition in mutant lines. M. P. and V. Ž. planned the
645 experiments and wrote the manuscript. T. P. performed root hair growth and callose
646 deposition analysis, prepared figures and wrote the manuscript.
647
648 **Acknowledgment**
649 We would like to thank to Norbert Zlámal from the Bratislava`s Comenius
650 University Botanical Garden for sharing *Selaginella uncinata*, Melanie Krebs (Uni
651 Heidelberg), Adriana Jelínková and Edita Janková Drdová (IEB CAS) for sharing
652 Arabidopsis mutants and markers seeds, and Jana Šťovíčková for technical assistance.
653 This work was supported by the Ministry of Education, Youth and Sports (MEYS)
654 project CZ.02.1.01/0.0/0.0/16_019/0000738, 8J19FR001 MEYS Czech-French mobility
655 program and Charles University Grant Agency (GAUK) project 415322. The Imaging
656 Facility of the Institute of Experimental Botany AS CR is supported by the MEYS CR
657 (LM2023050 Czech-BioImaging) and IEB AS CR.
658
659 **Legend to figures**
660 **Figure 1.** Concentration dependent modes of chitosan-triggered callose deposition.
661 Different concentrations of chitosan cause different patterns of callose depositions 24
662 h post treatment (p. t.) in both cotyledons and roots (root hairs); mock treatment as a
663 control below (bar = 100 μm). B) Concentration dependent primary root growth
664 inhibition 24 h p. t. n=8 - 11; small letters indicate significance of differences based on
665 the ANOVA test.
666 **Figure 2**. Root hair growth during the chitosan treatments. A) The low chitosan
667 concentration (0.001%, LCC) of several other chitosan variants has the same effect on
668 RH callose deposition (bar = 100 μm).
669 **Figure 3.** Callose deposition in LCC is PMR4-dependent. A) A *pmr4* mutant root hair
670 (RH) growth does not deposit callose upon the LCC treatment; nevertheless, the RH
671 growth is suppressed to the similar extent as in the Col-0 control. Small letters indicate
672 significance of differences based on the ANOVA test; n=100-140. B) Upon the LCC
673 treatment, at 4 h p. t. GFP-PMR4 accumulates in the tips of growing RH, further
674 confirming a role for PMR4 in RHs callose deposition (marked by white asterisks). C)
675 The appearance of root hairs of mock-treated (bright field, BF) and LCC-treated
676 (callose stained with aniline blue, AB) seedlings at 4, 8 and 12 h p. t. D) Timecourse of
677 the decline of the RH growth and the callose deposition reveals significant changes

678 between the mock- and LCC- treated seedlings in the growth observable at 12 h p.t.
679 (n=90-140), and in the callose deposition already at 4 h p. t. (n=20-35). Small letters
680 indicate significance of differences based on the ANOVA test. Bars = 100 μm in A), C)
681 and D) and 10 μm in B).
682 **Figure 4.** Chitosan-triggered signalling in *A. thaliana* seedlings. A) Ca^{2+} spiking
683 analysed as R-GECO1 sensor fluorescence in root cells upon chitosan treatment shows
684 slightly later onset with mild oscillations and long duration within the ca 45 min frame
685 of LCC treatment, while HCC induces prominent Ca^{2+} spiking with subsequent drop
686 in signal intensity. The error envelope represents SD, n=4-8. B) Western blot analysis
687 of MAPK activation by phosphorylation upon 30 min of HCC and LCC treatments
688 quantified as the ratio of band intensities obtained for phosphorylated portion versus
689 the whole pool MAPKs. Both treatments cause significant increase in MPK3/6/4
690 phosphorylation in comparison to the mock treatment, also the difference between the
691 LCC- and HCC-caused phosphorylations is significant, with LCC causing almost two-
692 time less MAPKs phosphorylation. Small letters indicate significance of differences
693 based on the ANOVA test, n=9. D) Bacteria Pst *hrcC* amplification in seedlings
694 pretreated with mock, HCC and LCC (24 h of pretreatment + 24 h of bacteria
695 inoculation); n=7-8, small letters indicate significance of differences based on the
696 ANOVA test.
697 **Figure 5.** R-GECO1 fluorescence patterns in RHs of treated seedlings. (A) represents
698 the root of 6-day-old seedling expressing R-GECO1 (an example of the red signal
699 appearance shown in upper left box), with indicated root hairs analysed in section (B)
700 (red dashed rectangle; RH1, RH2, RH3). Artificial LUTs (green fire blue) were used;
701 the calibration bar represents the signal intensity (box on the right). (B) shows R-
702 GECO1 oscillations depicted via kymograph throughout the experiment (Untreated,
703 mock, LCC, HCC) of 3 selected RH (RH1-3). White dashed lines indicate the end of a
704 particular part of the treatment, magenta dashed rectangle indicates the specific
705 oscillation pattern caused by flooding the sample with ½ MS solution. White brackets
706 indicate specific time windows used for the section (C). Section (C) represents 4 typical
707 R-GECO1 oscillation patterns for each treatment (Untr (untreated), mock, LCC, HCC)
708 visualised on 6 consecutive frames with 5 s gaps of RH1. Scale bar = 10 μm.
709 **Figure 6.** Subcellular dynamics during the early time points of LCC and HCC
710 treatments. A) The real-time analysis of the root hairs growth during the mock, LCC,
711 and HCC treatments based on the bright field images. The plot shows the RH growth
712 rates for the mock, LCC and HCC treatments; small letters indicate significant
713 differences based on Kruskal - Wallis test. B) The real-time changes in the vacuolar
714 dynamics quantified as a vacuole-occupied area in the RH tip, imaged using the

715 tonoplast marker Vti-GFP. The plot displays the differences between two consecutive
716 frames; the examples of the differential signal are shown on the right; examples of
717 vacuolar dynamics are shown below. Small letters indicate significant differences
718 based on the ANOVA test. Bar = 20 μm. C) The analyses of the endocytosed FM4-64
719 dye after 15 min of treatments for mock, LCC, and HCC. The endocytic compartment
720 stained by FM4-64 in the RH tip area is prominently enhanced in case of the HCC
721 treatments. Small letters indicate significant differences based on Kruskal -Wallis test.
722 On the right are examples of maximal intensity projections of FM4 -64 stained root
723 hairs. Bar = 10 μm.
724 **Figure 7.** Callose deposition is conserved in structures analogous to root hairs. *M.*
725 *polymorpha* (liverwort) rhizoids growing out of gemma are enclosed by callose when
726 incubated for 24 h with LCC. The same effect is observable also on spikemoss
727 rhizophores (*S. uncinata*). Bar = 100 μm.
728
729 **Table I.** Eleven genes (out of 58 DEGS; most of them with high RH expression) are
730 specifically affected by LCC, when compared to HCC (out of 8508 DEGs), as shown by
731 the RNAseq analysis performed on 6 d.o. plants cultivated in liquid medium (mock,
732 LCC, HCC; 24h); 5 genes below the line in the Table are differentially expressed in LCC
733 in comparison to HCC (fold change < 1 = downregulation, fold change > 1 =
734 upregulation).
735
736 **Supplementary figure 1.** A) Cultivation in water does not favour the RH growth and
737 callose deposition; the RH callose reaction requires a rich cultivation medium in order
738 for RHs to grow, and callose deposits to be formed. B) The growth of new RH is
739 inhibited in early time points (4 and 8 h p. t.) in high chitosan concentration (HCC;
740 bars = 100 μm). C) Arabidopsis mutants in secretion, defence and phytohormone
741 signalling have ability to deposit root hair callose similarly to WT/Col-0. Bars = 100
742 μm.
743 **Supplementary figure 2**. Actin dynamics is not significantly altered during the early
744 time points of the HCC treatment, as observed using fimbrin-GFP marker and
745 quantified using the variance between the two time points during the observation;
746 images on the right show examples of 5 consecutive frames for the two treatments.
747 **Supplementary figure 3. A)** Numbers of **s**pecific and common DEGs among three
748 different types of experiments with chitosan treatments. B) Cell wall changes triggered
749 by LCC treatment. Enzymatic fingerprinting of homogalacturonans (upper graph) and
750 xyloglucans (lower graph) from cell walls of WT mock and LCC treated leaves. Data
751 represents mean ±SD, n=4, *P<0.05, **P<0.01, student's t test. OGs are named

752 GalAxMeyAcz. x, y and z indicate the DP and the number of methyl- and acetylester
753 groups, respectively. GalA: Galacturonic acid, Me: methylester group, Ac: Acetylester
754 group. Xyloglucan fragment nomenclature follows that described in Fry et al. (1993):
755 G stands for glucose; X for xylose-glucose; L for galactose-xylose-glucose; F for fucose-
756 galactose-xylose-glucose.
757 **Supplementary figure 4.** Chitosan LCC treatment induces deposition of callose in
758 moss *P. patens* regenerating protoplasts (A) but not in leaf mesophyll-derived
759 Arabidopsis regenerating protoplasts (B), as assayed by aniline blue staining. Bars =
760 100 μm.
761 **Supplemental figure 5** LCC has a minor effect on auxin signalling enhancement as
762 demonstrated using the DR5::GFP reporter line (bar = 100 μm).
763

Bibliography

Aslam SN, Erbs G, Morrissey KL, Newman M-A, Chinchilla D, Boller T, Molinaro A, Jackson RW, Cooper RM. 2009. Microbe-associated molecular pattern (MAMP) signatures, synergy, size and charge: influences on perception or mobility and host defence responses. *Mol Plant Pathol* **10**:375–387. doi:10.1111/j.1364-3703.2009.00537.x

Badri DV, Loyola-Vargas VM, Du J, Stermitz FR, Broeckling CD, Iglesias-Andreu L, Vivanco JM. 2008. Transcriptome analysis of Arabidopsis roots treated with signaling compounds: A focus on signal transduction, metabolic regulation and secretion. *New Phytol* **179**:209–223. doi:10.1111/j.1469-8137.2008.02458.x

Baluška F, Salaj J, Mathur J, Braun M, Jasper F, Šamaj J, Chua NH, Barlow PW, Volkmann D. 2000. Root hair formation: F-actin-dependent tip growth is initiated by local assembly of profilin-supported F-actin meshworks accumulated within expansin-enriched bulges. *Dev Biol* **227**:618–632. doi:10.1006/dbio.2000.9908

Bennett MJ, Marchant A, Green HG, May ST, Ward SP, Millner PA, Walker AR, Schulz B, Feldmann KA. 1996. Arabidopsis AUX1 gene: a permease-like regulator of root gravitropism. *Science* **273**:948–950. doi:10.1126/science.273.5277.948

Brejšková L, Hála M, Rawat A, Soukupová H, Cvrčková F, Charlot F, Nogué F, Haluška S, Žárský V. 2021. SEC6 exocyst subunit contributes to multiple steps of growth and development of Physcomitrella (Physcomitrium patens). *Plant J* **106**:831–843. doi:10.1111/tpj.15205

Brost C, Studtrucker T, Reimann R, Denninger P, Czekalla J, Krebs M, Fabry B, Schumacher K, Grossmann G, Dietrich P. 2019. Multiple cyclic nucleotide-gated channels coordinate calcium oscillations and polar growth of root hairs. *Plant J Cell Mol Biol* **99**:910–923. doi:10.1111/tpj.14371

Cai G, Faleri C, Del Casino C, Emons AMC, Cresti M. 2011. Distribution of callose synthase, cellulose synthase, and sucrose synthase in tobacco pollen tube is controlled in dissimilar ways by actin filaments and microtubules. *Plant Physiol* **155**:1169–1190. doi:10.1104/pp.110.171371

Cao H, Bowling SA, Gordon AS, Dong X. 1994. Characterization of an Arabidopsis Mutant That Is Nonresponsive to Inducers of Systemic Acquired Resistance. *Plant Cell* **6**:1583–1592. doi:10.1105/tpc.6.11.1583

Cao Y, Liang Y, Tanaka K, Nguyen CT, Jedrzejczak RP, Joachimiak A, Stacey G. 2014. The kinase LYK5 is a major chitin receptor in Arabidopsis and forms a chitin-induced complex with related kinase CERK1. *eLife* **3**:e03766. doi:10.7554/eLife.03766

Carol RJ, Dolan L. 2002. Building a hair: tip growth in Arabidopsis thaliana root hairs. *Philos Trans R*

Soc Lond B Biol Sci **357**:815–821. doi:10.1098/rstb.2002.1092
Cavalier DM, Lerouxel O, Neumetzler L, Yamauchi K, Reinecke A, Freshour G, Zabotina OA, Hahn MG, Burgert I, Pauly M, Raikhel NV, Keegstra K. 2008. Disrupting two Arabidopsis thaliana xylosyltransferase genes results in plants deficient in xyloglucan, a major primary cell wall component. *Plant Cell* **20**:1519–1537. doi:10.1105/tpc.108.059873
Chin K, DeFalco TA, Moeder W, Yoshioka K. 2013. The Arabidopsis cyclic nucleotide-gated ion channels AtCNGC2 and AtCNGC4 work in the same signaling pathway to regulate pathogen defense and floral transition. *Plant Physiol* **163**:611–624. doi:10.1104/pp.113.225680
Chuberre C, Plancot B, Driouich A, Moore JP, Bardor M, Gügi B, Vicré M. 2018. Plant immunity is compartmentalized and specialized in roots. *Front Plant Sci* **871**:1692–1692. doi:10.3389/fpls.2018.01692
Cove DJ, Perroud P-F, Charron AJ, McDaniel SF, Khandelwal A, Quatrano RS. 2009. Culturing the moss Physcomitrella patens. *Cold Spring Harb Protoc* **2009**:pdb.prot5136. doi:10.1101/pdb.prot5136
Cui W, Lee J-Y. 2016. Arabidopsis callose synthases CalS1/8 regulate plasmodesmal permeability during stress. *Nat Plants* **2**:16034. doi:10.1038/nplants.2016.34
Dehors J, Mareck A, Kiefer-Meyer M-C, Menu-Bouaouiche L, Lehner A, Mollet J-C. 2019. Evolution of Cell Wall Polymers in Tip-Growing Land Plant Gametophytes: Composition, Distribution, Functional Aspects and Their Remodeling. *Front Plant Sci* **10**:441. doi:10.3389/fpls.2019.00441
Denoux C, Galletti R, Mammarella N, Gopalan S, Werck D, De Lorenzo G, Ferrari S, Ausubel FM, Dewdney J. 2008. Activation of defense response pathways by OGs and Flg22 elicitors in Arabidopsis seedlings. *Mol Plant* **1**:423–445. doi:10.1093/mp/ssn019
Dolan L. 1996. Pattern in the root epidermis: An interplay of diffusible signals and cellular geometry. *Ann Bot* **77**:547–553. doi:10.1006/anbo.1996.0069
Epel BL. 2009. Plant viruses spread by diffusion on ER-associated movement-protein-rafts through plasmodesmata gated by viral induced host beta-1,3-glucanases. *Semin Cell Dev Biol* **20**:1074–1081. doi:10.1016/j.semcdb.2009.05.010
Fernandez AI, Beeckman T. 2020. An MAP Kinase Cascade Downstream of RGF/GLV Peptides and Their RGI Receptors Regulates Root Development. *Mol Plant* **13**:1542–1544. doi:10.1016/j.molp.2020.10.009
Galway ME, Eng RC, Schiefelbein JW, Wasteneys GO. 2011. Root hair-specific disruption of cellulose and xyloglucan in AtCSLD3 mutants, and factors affecting the post-rupture resumption of mutant root hair growth. *Planta* **233**:985–999. doi:10.1007/s00425-011-1355-6
Gamborg OL, Miller RA, Ojima K. 1968. Nutrient requirements of suspension cultures of soybean root cells. *Exp Cell Res* **50**:151–158. doi:10.1016/0014-4827(68)90403-5
German L, Yeshvekar R, Benitez-Alfonso Y. 2023. Callose metabolism and the regulation of cell walls and plasmodesmata during plant mutualistic and pathogenic interactions. *Plant Cell Environ* **46**:391–404. doi:10.1111/pce.14510
Gómez-Gómez L, Felix G, Boller T. 1999. A single locus determines sensitivity to bacterial flagellin in Arabidopsis thaliana. *Plant J Cell Mol Biol* **18**:277–284. doi:10.1046/j.1365-313x.1999.00451.x
Heisler MG, Ohno C, Das P, Sieber P, Reddy GV, Long JA, Meyerowitz EM. 2005. Patterns of auxin transport and gene expression during primordium development revealed by live imaging of the Arabidopsis inflorescence meristem. *Curr Biol CB* **15**:1899–1911. doi:10.1016/j.cub.2005.09.052
Herburger K, Holzinger A. 2015. Localization and Quantification of Callose in the Streptophyte Green Algae Zygnema and Klebsormidium: Correlation with Desiccation Tolerance. *Plant Cell Physiol* **56**:2259–2270. doi:10.1093/pcp/pcv139
Ichikawa M, Hirano T, Enami K, Fuselier T, Kato N, Kwon C, Voigt B, Schulze-Lefert P, Baluška F, Sato MH. 2014. Syntaxin of plant proteins SYP123 and SYP132 mediate root hair tip growth in Arabidopsis thaliana. *Plant Cell Physiol* **55**:790–800. doi:10.1093/pcp/pcu048
Iriti M, Sironi M, Gomarasca S, Casazza AP, Soave C, Faoro F. 2006. Cell death-mediated antiviral

effect of chitosan in tobacco. *Plant Physiol Biochem PPB* **44**:893–900. doi:10.1016/j.plaphy.2006.10.009

Ishiga Y, Ishiga T, Uppalapati SR, Mysore KS. 2011. Arabidopsis seedling flood-inoculation technique: a rapid and reliable assay for studying plant-bacterial interactions. *Plant Methods* **7**:32. doi:10.1186/1746-4811-7-32

Jacobs AK, Lipka V, Burton RA, Panstruga R, Strizhov N, Schulze-Lefert P, Fincher GB. 2003. An Arabidopsis Callose Synthase, GSL5, Is Required for Wound and Papillary Callose Formation. *Plant Cell* **15**:2503–2513. doi:10.1105/tpc.016097

Jones JDG, Dangl JL. 2006. The plant immune system. *Nature* **444**:323–329. doi:10.1038/nature05286

Keinath NF, Waadt R, Brugman R, Schroeder JI, Grossmann G, Schumacher K, Krebs M. 2015. Live Cell Imaging with R-GECO1 Sheds Light on flg22- and Chitin-Induced Transient [Ca2+]cyt Patterns in Arabidopsis. *Mol Plant* **8**:1188–1200. doi:10.1016/j.molp.2015.05.006

Kemmerling B, Schwedt A, Rodriguez P, Mazzotta S, Frank M, Qamar SA, Mengiste T, Betsuyaku S, Parker JE, Müssig C, Thomma BPHJ, Albrecht C, de Vries SC, Hirt H, Nürnberger T. 2007. The BRI1-associated kinase 1, BAK1, has a brassinolide-independent role in plant cell-death control. *Curr Biol CB* **17**:1116–1122. doi:10.1016/j.cub.2007.05.046

Kentaro Okada, Koei Yachi, Tan Anh Nhi Nguyen, Satomi Kanno, Chika Tateda, Tae-Hong Lee, Uyen Nguyen, Shunsuke Miyashima, Kei Hiruma, Kyoko Miwa, Takaki Maekawa, Michitaka Notaguchi, Yusuke Saijo. 2023. Defense-related callose synthase PMR4 promotes root hair callose deposition and adaptation to phosphate deficiency in Arabidopsis thaliana. *bioRxiv* 2023.07.05.547890. doi:10.1101/2023.07.05.547890

Ks R, Ra L, Rd W, Ha O, A M. 2020. Callose in sporogenesis: Novel composition of the inner spore wall in hornworts. *Plant Syst Evol Entwicklungsgeschichte Syst Pflanz* **306**:16. doi:10.1007/s00606-020-01631-5

Kubátová Z, Pejchar P, Potocký M, Sekereš J, Žárský V, Kulich I. 2019. Arabidopsis Trichome Contains Two Plasma Membrane Domains with Different Lipid Compositions Which Attract Distinct EXO70 Subunits. *Int J Mol Sci* **20**:3803. doi:10.3390/ijms20153803

Kulich I, Vojtíková Z, Glanc M, Ortmannová J, Rasmann S, Žárský V. 2015. Cell wall maturation of Arabidopsis trichomes is dependent on exocyst subunit EXO70H4 and involves callose deposition. *Plant Physiol* **168**:120–131. doi:10.1104/pp.15.00112

Kulich I, Vojtíková Z, Sabol P, Ortmannová J, Neděla V, Tihlaříková E, Žárský V. 2018. Exocyst Subunit EXO70H4 Has a Specific Role in Callose Synthase Secretion and Silica Accumulation. *Plant Physiol* **176**:2040–2051. doi:10.1104/pp.17.01693

Ladwig F, Dahlke RI, Stührwohldt N, Hartmann J, Harter K, Sauter M. 2015. Phytosulfokine regulates growth in arabidopsis through a response module at the plasma membrane that includes cyclic nucleotide-gated channel17, H+-ATPase, and BAK1. *Plant Cell* **27**:1718–1729. doi:10.1105/tpc.15.00306

Lopez-Moya F, Escudero N, Zavala-Gonzalez EA, Esteve-Bruna D, Blázquez MA, Alabadí D, Lopez-Llorca LV. 2017. Induction of auxin biosynthesis and WOX5 repression mediate changes in root development in Arabidopsis exposed to chitosan. *Sci Rep* **7**:16813. doi:10.1038/s41598-017-16874-5

Luna E, Pastor V, Robert J, Flors V, Mauch-Mani B, Ton J. 2011. Callose deposition: a multifaceted plant defense response. *Mol Plant-Microbe Interact MPMI* **24**:183–193. doi:10.1094/MPMI-07-10-0149

Ma X, Wu Y, Zhang G. 2021. Formation pattern and regulatory mechanisms of pollen wall in Arabidopsis. *J Plant Physiol* **260**:153388. doi:10.1016/j.jplph.2021.153388

Meyer D, Pajonk S, Micali C, O'Connell R, Schulze-Lefert P. 2009. Extracellular transport and integration of plant secretory proteins into pathogen-induced cell wall compartments. *Plant J Cell Mol Biol* **57**:986–999. doi:10.1111/j.1365-313X.2008.03743.x

Millet YA, Danna CH, Clay NK, Songnuan W, Simon MD, Werck-Reichhart D, Ausubel FM. 2010. Innate immune responses activated in Arabidopsis roots by microbe-associated molecular patterns. *Plant Cell* **22**:973–990. doi:10.1105/tpc.109.069658

Miya A, Albert P, Shinya T, Desaki Y, Ichimura K, Shirasu K, Narusaka Y, Kawakami N, Kaku H, Shibuya N. 2007. CERK1, a LysM receptor kinase, is essential for chitin elicitor signaling in Arabidopsis. *Proc Natl Acad Sci U S A* **104**:19613–19618. doi:10.1073/pnas.0705147104

Motomura K, Sugi N, Takeda A, Yamaoka S, Maruyama D. 2022. Possible molecular mechanisms of persistent pollen tube growth without de novo transcription. *Front Plant Sci* **13**:1020306. doi:10.3389/fpls.2022.1020306

Ngou BPM, Ahn H-K, Ding P, Jones JDG. 2021. Mutual potentiation of plant immunity by cell-surface and intracellular receptors. *Nature* **592**:110–115. doi:10.1038/s41586-021-03315-7

Okada K, Kubota Y, Hirase T, Otani K, Goh T, Hiruma K, Saijo Y. 2021. Uncoupling root hair formation and defence activation from growth inhibition in response to damage-associated Pep peptides in Arabidopsis thaliana. *New Phytol* **229**:2844–2858. doi:10.1111/nph.17064

Ortmannová J, Sekereš J, Kulich I, Šantrůček J, Dobrev P, Žárský V, Pečenková T. 2022. Arabidopsis EXO70B2 exocyst subunit contributes to papillae and encasement formation in antifungal defence. *J Exp Bot* **73**:742–755. doi:10.1093/jxb/erab457

Park K, Jang BK, Lee HM, Cho JS, Lee CH. 2020. An Efficient Method for In Vitro Shoot-Tip Culture and Sporophyte Production Using Selaginella martensii Spring Sporophyte. *Plants Basel Switz* **9**:235. doi:10.3390/plants9020235

Park S, Szumlanski AL, Gu F, Guo F, Nielsen E. 2011. A role for CSLD3 during cell-wall synthesis in apical plasma membranes of tip-growing root-hair cells. *Nat Cell Biol* **13**:973–980. doi:10.1038/ncb2294

Parker JS, Cavell AC, Dolan L, Roberts K, Grierson CS. 2000. Genetic interactions during root hair morphogenesis in Arabidopsis. *Plant Cell* **12**:1961–1974. doi:10.1105/tpc.12.10.1961

Paterlini A, Sechet J, Immel F, Grison MS, Pilard S, Pelloux J, Mouille G, Bayer EM, Voxeur A. 2022. Enzymatic fingerprinting reveals specific xyloglucan and pectin signatures in the cell wall purified with primary plasmodesmata. *Front Plant Sci* **13**.

Pečenková T, Janda M, Ortmannová J, Hajná V, Stehlíková Z, Žárský V. 2017. Early Arabidopsis root hair growth stimulation by pathogenic strains of Pseudomonas syringae. *Ann Bot* **120**:437–446. doi:10.1093/aob/mcx073

Pečenková T, Potocká A, Potocký M, Ortmannová J, Drs M, Janková Drdová E, Pejchar P, Synek L, Soukupová H, Žárský V, Cvrčková F. 2020. Redundant and Diversified Roles Among Selected Arabidopsis thaliana EXO70 Paralogs During Biotic Stress Responses. *Front Plant Sci* **11**:960–960. doi:10.3389/fpls.2020.00960

Porter K, Day B. 2016. From filaments to function: The role of the plant actin cytoskeleton in pathogen perception, signaling and immunity. *J Integr Plant Biol* **58**:299–311. doi:10.1111/jipb.12445

Radin I, Richardson RA, Coomey JH, Weiner ER, Bascom CS, Li T, Bezanilla M, Haswell ES. 2021. Plant PIEZO homologs modulate vacuole morphology during tip growth. *Science* **373**:586–590. doi:10.1126/science.abe6310

Rentel MC, Lecourieux D, Ouaked F, Usher SL, Petersen L, Okamoto H, Knight H, Peck SC, Grierson CS, Hirt H, Knight MR. 2004. OXI1 kinase is necessary for oxidative burst-mediated signalling in Arabidopsis. *Nature* **427**:858–861. doi:10.1038/nature02353

Rich-Griffin C, Eichmann R, Reitz MU, Hermann S, Woolley-Allen K, Brown PE, Wiwatdirekkul K, Esteban E, Pasha A, Kogel KH, Provart NJ, Ott S, Schäfer P. 2020. Regulation of cell type-specific immunity networks in arabidopsis roots. *Plant Cell* **32**:2742–2762. doi:10.1105/TPC.20.00154

Ringli C, Baumberger N, Diet A, Frey B, Keller B. 2002. ACTIN2 is essential for bulge site selection and tip growth during root hair development of Arabidopsis. *Plant Physiol* **129**:1464–1472. doi:10.1104/pp.005777

Serre NBC, Kralík D, Yun P, Slouka Z, Shabala S, Fendrych M. 2021. AFB1 controls rapid auxin signalling through membrane depolarization in Arabidopsis thaliana root. *Nat Plants* **7**:1229–1238. doi:10.1038/s41477-021-00969-z

Shih HW, Depew CL, Miller ND, Monshausen GB. 2015. The cyclic nucleotide-gated channel CNGC14

regulates root gravitropism in arabidopsis thaliana. *Curr Biol* **25**:3119–3125. doi:10.1016/j.cub.2015.10.025
Sun H, Zhu X, Li C, Ma Z, Han X, Luo Y, Yang L, Yu J, Miao Y. 2021. Xanthomonas effector XopR hijacks host actin cytoskeleton via complex coacervation. *Nat Commun* **12**:4064. doi:10.1038/s41467-021-24375-3
Suwanchaikasem P, Idnurm A, Selby-Pham J, Walker R, Boughton BA. 2022. Root-TRAPR: a modular plant growth device to visualize root development and monitor growth parameters, as applied to an elicitor response of Cannabis sativa. *Plant Methods* **18**:46. doi:10.1186/s13007-022-00875-1
Vaškebová L, Šamaj J, Ovecka M. 2018. Single-point ACT2 gene mutation in the Arabidopsis root hair mutant der1-3 affects overall actin organization, root growth and plant development. *Ann Bot* **122**:889–901. doi:10.1093/aob/mcx180
Verma DP, Hong Z. 2001. Plant callose synthase complexes. *Plant Mol Biol* **47**:693–701. doi:10.1023/a:1013679111111
Vissenberg K, Claeijs N, Balcerowicz D, Schoenaers S. 2020. Hormonal regulation of root hair growth and responses to the environment in Arabidopsis. *J Exp Bot* **71**:2412–2427. doi:10.1093/JXB/ERAA048
Vogel J, Somerville S. 2000. Isolation and characterization of powdery mildew-resistant Arabidopsis mutants. *Proc Natl Acad Sci U S A* **97**:1897–1902. doi:10.1073/pnas.030531997
Voxeur A, Habrylo O, Guénin S, Miart F, Soulié M-C, Rihouey C, Pau-Roblot C, Domon J-M, Gutierrez L, Pelloux J, Mouille G, Fagard M, Höfte H, Vernhettes S. 2019. Oligogalacturonide production upon Arabidopsis thaliana-Botrytis cinerea interaction. *Proc Natl Acad Sci U S A* **116**:19743–19752. doi:10.1073/pnas.1900317116
Wan J, Tanaka K, Zhang X-C, Son GH, Brechenmacher L, Nguyen THN, Stacey G. 2012. LYK4, a lysin motif receptor-like kinase, is important for chitin signaling and plant innate immunity in Arabidopsis. *Plant Physiol* **160**:396–406. doi:10.1104/pp.112.201699
Wang X, Wang K, Yin G, Liu X, Liu M, Cao N, Duan Y, Gao H, Wang W, Ge W, Wang J, Li R, Guo Y. 2018. Pollen-Expressed Leucine-Rich Repeat Extensins Are Essential for Pollen Germination and Growth. *Plant Physiol* **176**:1993–2006. doi:10.1104/pp.17.01241
Wang Y-S, Motes CM, Mohamalawari DR, Blancaflor EB. 2004. Green fluorescent protein fusions to Arabidopsis fimbrin 1 for spatio-temporal imaging of F-actin dynamics in roots. *Cell Motil Cytoskeleton* **59**:79–93. doi:10.1002/cm.20024
Ye W, Munemasa S, Shinya T, Wu W, Ma T, Lu J, Kinoshita T, Kaku H, Shibuya N, Murata Y. 2020. Stomatal immunity against fungal invasion comprises not only chitin-induced stomatal closure but also chitosan-induced guard cell death. *Proc Natl Acad Sci U S A* **117**:20932–20942. doi:10.1073/pnas.1922319117
Yoo S-D, Cho Y-H, Sheen J. 2007. Arabidopsis mesophyll protoplasts: a versatile cell system for transient gene expression analysis. *Nat Protoc* **2**:1565–1572. doi:10.1038/nprot.2007.199
Yuan P, Jauregui E, Du L, Tanaka K, Poovaiah BW. 2017. Calcium signatures and signaling events orchestrate plant–microbe interactions. *Curr Opin Plant Biol* **38**:173–183. doi:10.1016/j.pbi.2017.06.003
Zamioudis C, Mastranesti P, Dhonukshe P, Blilou I, Pieterse CMJ. 2013. Unraveling root developmental programs initiated by beneficial Pseudomonas spp. Bacteria. *Plant Physiol* **162**:304–318. doi:10.1104/pp.112.212597
Zhang J, Li Y, Bao Q, Wang H, Hou S. 2022. Plant elicitor peptide 1 fortifies root cell walls and triggers a systemic root-to-shoot immune signaling in Arabidopsis. *Plant Signal Behav* **17**:2034270. doi:10.1080/15592324.2022.2034270
Zhang M, Zhang S. 2022. Mitogen-activated protein kinase cascades in plant signaling. *J Integr Plant Biol* **64**:301–341. doi:10.1111/jipb.13215

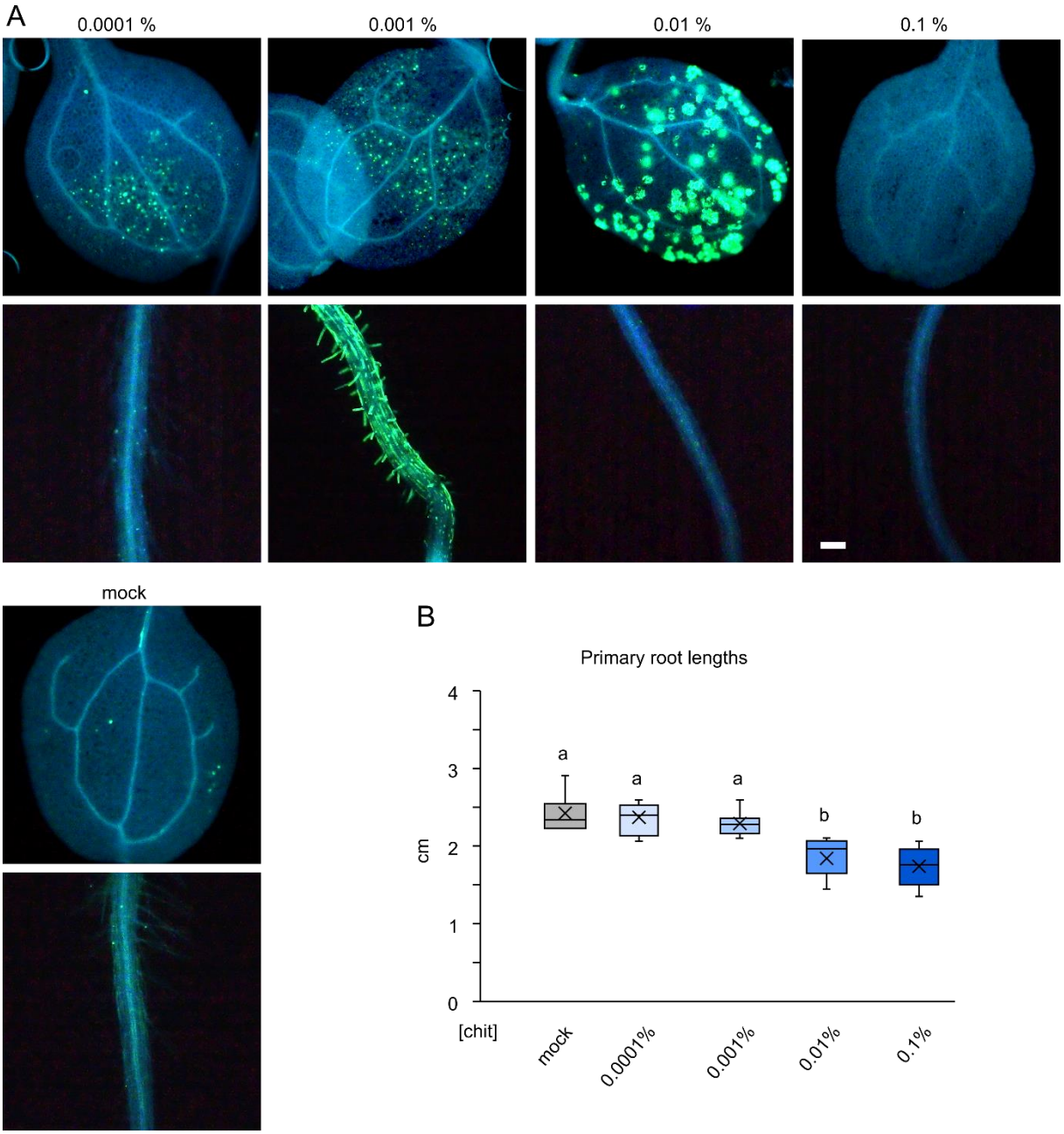

Figure 1. Concentration dependent modes of chitosan-triggered callose deposition. Different concentrations of chitosan cause different patterns of callose depositions 24 h post treatment (p. t.) in both cotyledons and roots (root hairs); mock treatment as a control below (bar = 100 µm). B) Concentration dependent primary root growth inhibition 24 h p. t. n=8 - 11; small letters indicate significance of differences based on the ANOVA test.

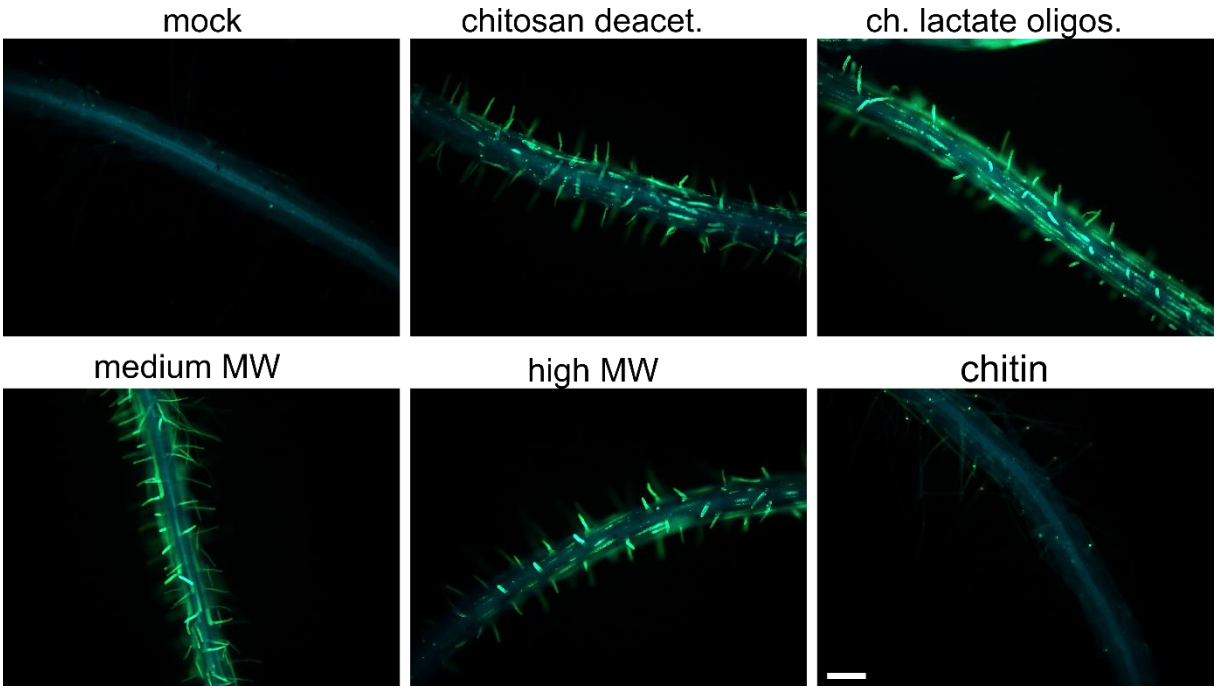

Figure 2. Root hair growth during the chitosan treatments. A) The low chitosan concentration (0.001%, LCC) of several other chitosan variants has the same effect on RH callose deposition (bar = 100 μm).

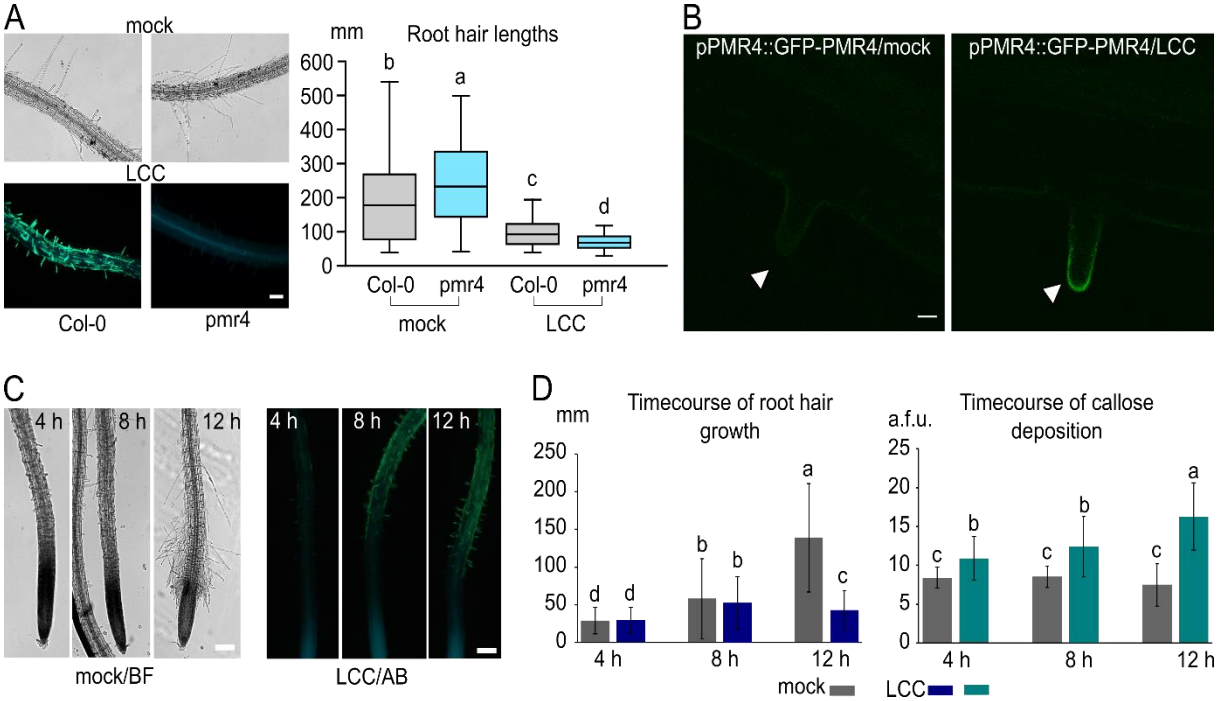

Figure 3. Callose deposition in LCC is PMR4-dependent. A) A *pmr4* mutant root hair (RH) growth does not deposit callose upon the LCC treatment; nevertheless, the RH growth is suppressed to the similar extent as in the Col-0 control. Small letters indicate significance of differences based on the ANOVA test; n=100-140. B) Upon the LCC treatment, at 4 h p. t. GFP-PMR4 accumulates in the tips of growing RH, further confirming a role for PMR4 in RHs callose deposition (marked by white asterisks). C) The appearance of root hairs of mock-treated (bright field, BF) and LCC-treated (callose stained with aniline blue, AB) seedlings at 4, 8 and 12 h p. t. D) Timecourse of the decline of the RH growth and the callose deposition reveals significant changes between the mock- and LCC- treated seedlings in the growth observable at 12 h p.t. (n=90-140), and in the callose deposition already at 4 h p. t. (n=20-35). Small letters indicate significance of differences based on the ANOVA test. Bars = 100 μm in A), C) and D) and 10 μm in B).

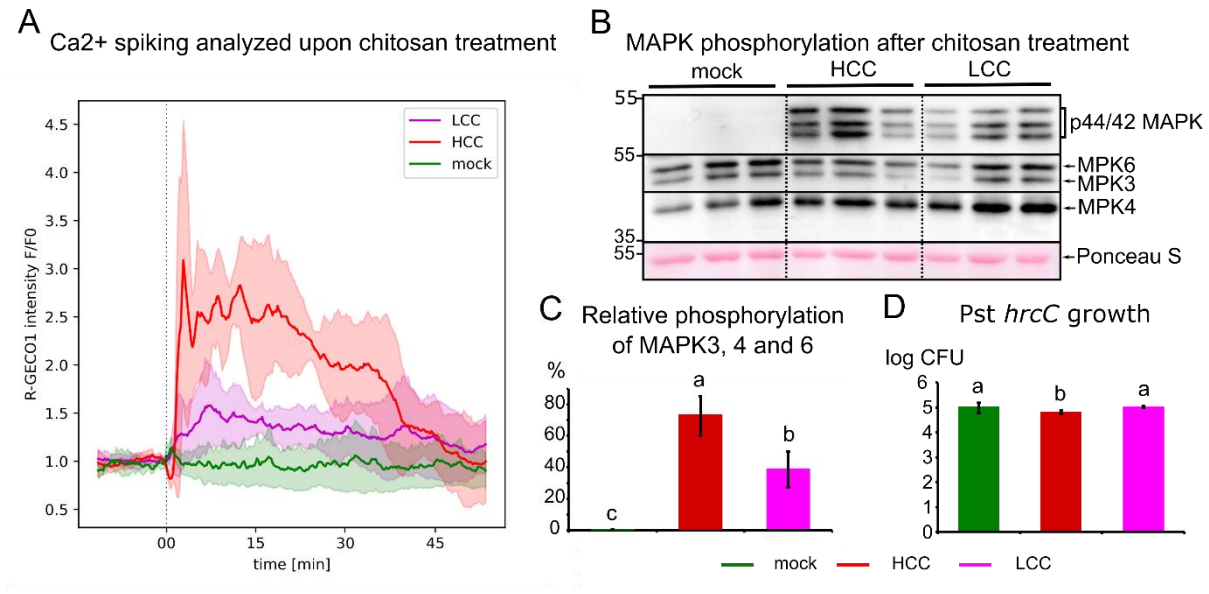

Figure 4. Chitosan-triggered signalling in *A. thaliana* seedlings. A) Ca^{2+} spiking analysed as R-GECO1 sensor fluorescence in root cells upon chitosan treatment shows slightly later onset with mild oscillations and long duration within the ca 45 min frame of LCC treatment, while HCC induces prominent Ca^{2+} spiking with subsequent drop in signal intensity. The error envelope represents SD, n=4-8. B) Western blot analysis of MAPK activation by phosphorylation upon 30 min of HCC and LCC treatments quantified as the ratio of band intensities obtained for phosphorylated portion versus the whole pool MAPKs. Both treatments cause significant increase in MPK3/6/4 phosphorylation in comparison to the mock treatment, also the difference between the LCC- and HCC-caused phosphorylations is significant, with LCC causing almost two-time less MAPKs phosphorylation. Small letters indicate significance of differences based on the ANOVA test, n=9. D) Bacteria Pst *hrcC* amplification in seedlings pretreated with mock, HCC and LCC (24 h of pretreatment + 24 h of bacteria inoculation); n=7-8, small letters indicate significance of differences based on the ANOVA test.

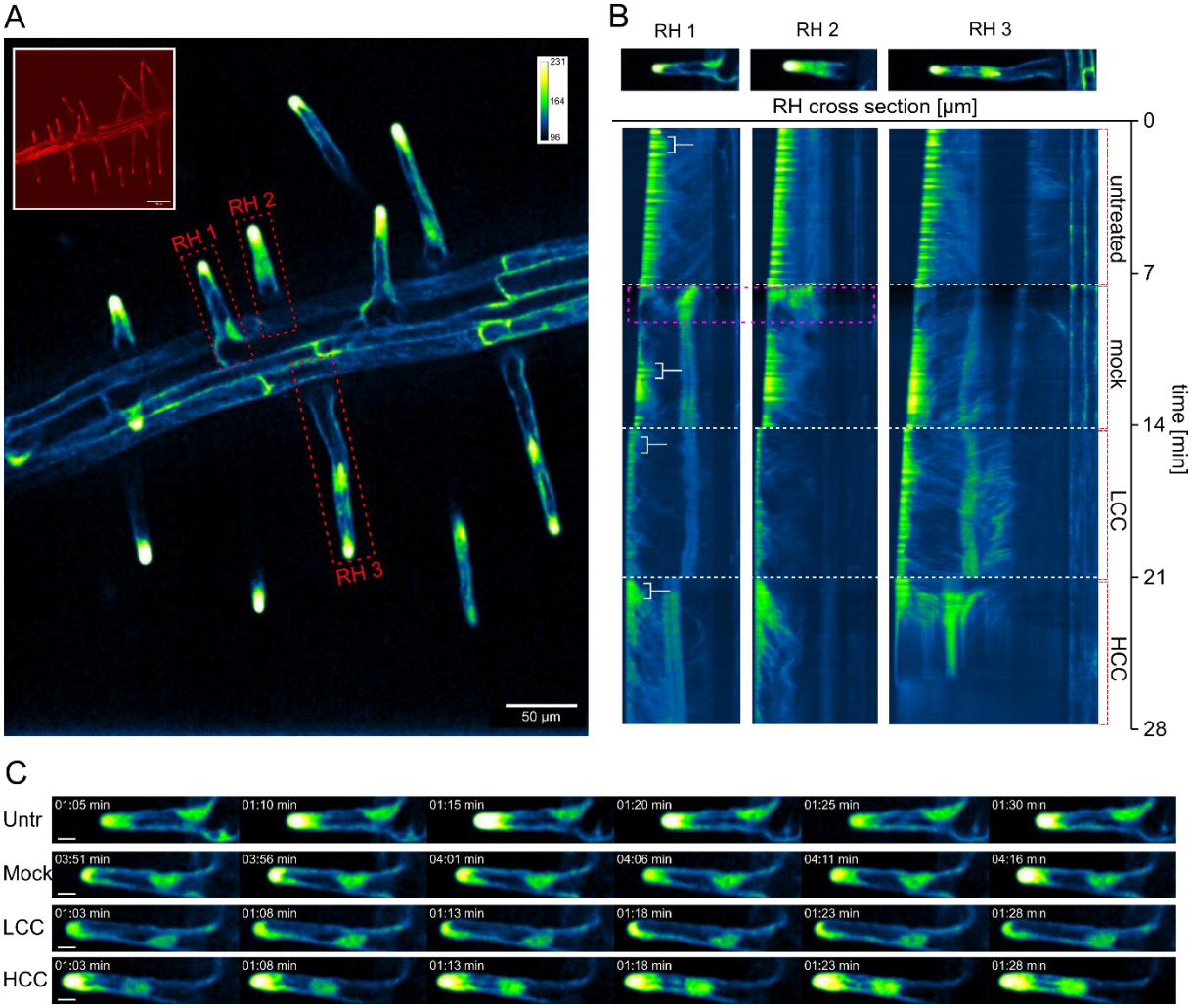

Figure 5. R-GECO1 fluorescence patterns in RHs of treated seedlings. (A) represents the root of 6-day-old seedling expressing R-GECO1 (an example of the red signal appearance shown in upper left box), with indicated root hairs analysed in section (B) (red dashed rectangle; RH1, RH2, RH3). Artificial LUTs (green fire blue) were used; the calibration bar represents the signal intensity (box on the right). (B) shows R-GECO1 oscillations depicted via kymograph throughout the experiment (Untreated, mock, LCC, HCC) of 3 selected RH (RH1-3). White dashed lines indicate the end of a particular part of the treatment, magenta dashed rectangle indicates the specific oscillation pattern caused by flooding the sample with ½ MS solution. White brackets indicate specific time windows used for the section (C). Section (C) represents 4 typical R-GECO1 oscillation patterns for each treatment (Untr (untreated), mock, LCC, HCC) visualised on 6 consecutive frames with 5 s gaps of RH1. Scale bar = 10 µm.

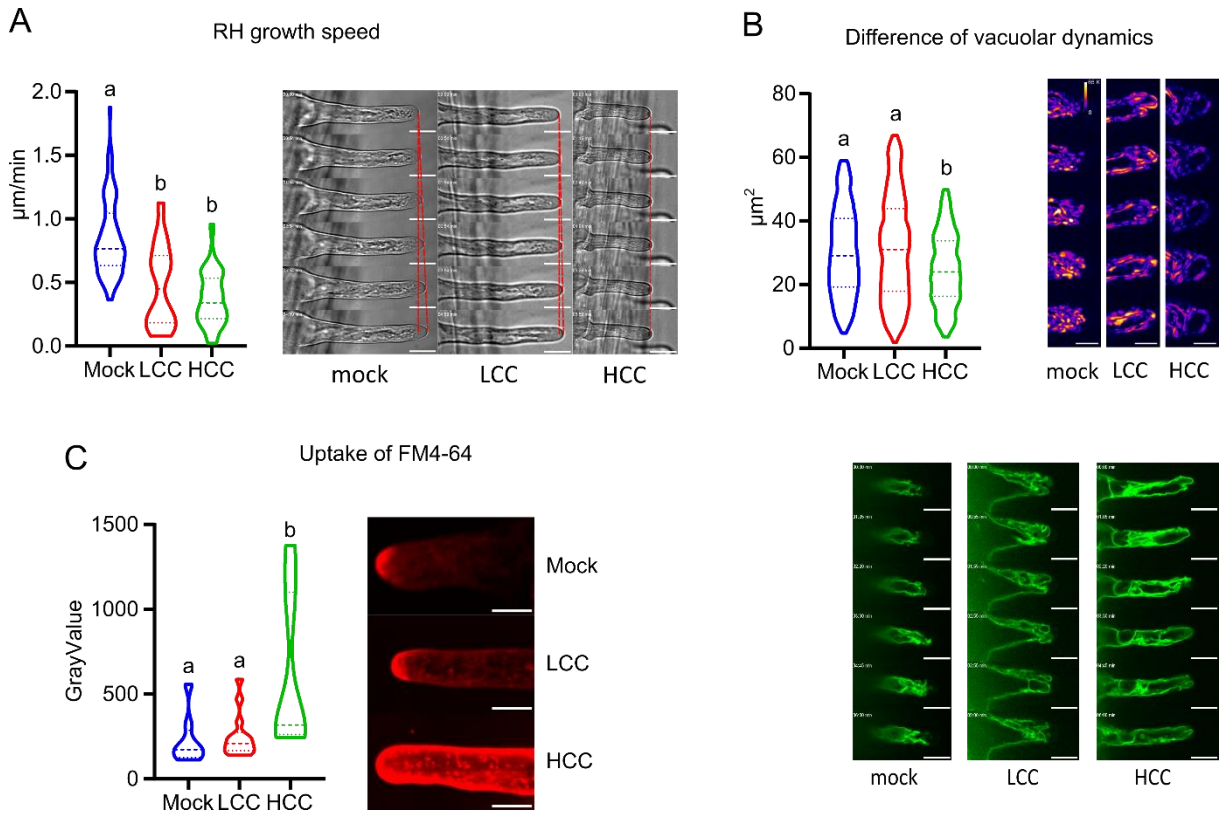

Figure 6. Subcellular dynamics during the early time points of LCC and HCC treatments. A) The real-time analysis of the root hairs growth during the mock, LCC, and HCC treatments based on the bright field images. The plot shows the RH growth rates for the mock, LCC and HCC treatments; small letters indicate significant differences based on Kruskal - Wallis test. B) The real-time changes in the vacuolar dynamics quantified as a vacuole-occupied area in the RH tip, imaged using the tonoplast marker Vti-GFP. The plot displays the differences between two consecutive frames; the examples of the differential signal are shown on the right; examples of vacuolar dynamics are shown below. Small letters indicate significant differences based on the ANOVA test. Bar = 20 µm. C) The analyses of the endocytosed FM4-64 dye after 15 min of treatments for mock, LCC, and HCC. The endocytic compartment stained by FM4-64 in the RH tip area is prominently enhanced in case of the HCC treatments. Small letters indicate significant differences based on Kruskal -Wallis test. On the right are examples of maximal intensity projections of FM4 -64 stained root hairs. Bar = 10 µm.

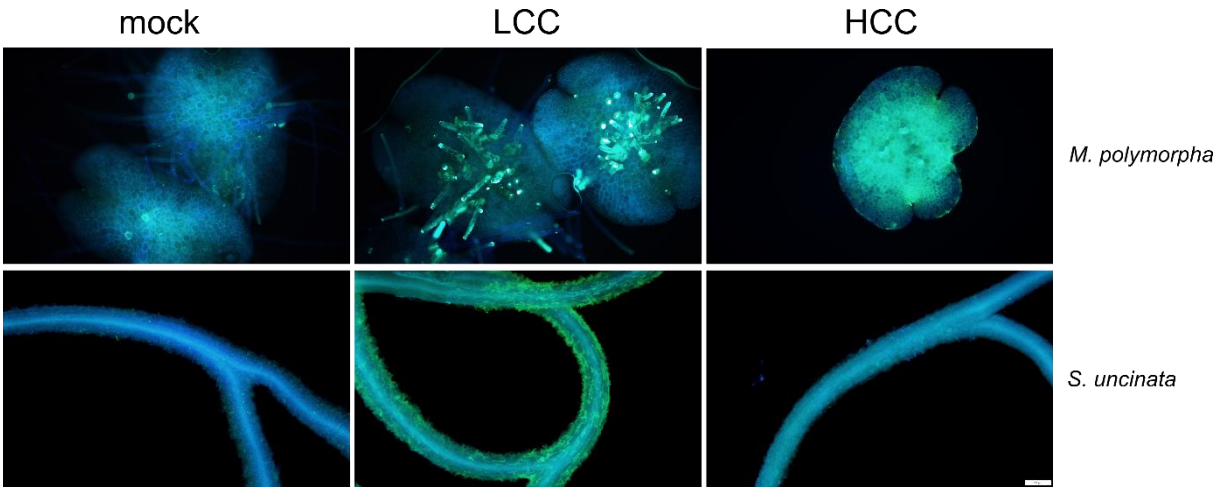

Figure 7. Callose deposition is conserved in structures analogous to root hairs. *M. polymorpha* (liverwort) rhizoids growing out of gemma are enclosed by callose when incubated for 24 h with LCC. The same effect is observable also on spikemoss rhizophores (*S. uncinata*). Bar = 100 μm.

Table I. Eleven genes (out of 59 DEGS; most of them with good RH expression) are specifically affected by LCC, when compared to HCC chitosan treatment (out of 8508 DEGs); 5 genes below the line in the Table are differentially expressed in LCC in comparison to HCC (fold change < 1 = downregulation, fold change > 1 = upregulation).

gene identifier	gene name	protein function	fold change LCC	fold change HCC
AT1G72900	ERF11	ERF domain protein 11	0.49	insig.
AT2G22500	DIC1	uncoupling protein 5	0.59	insig.
AT2G46400	WRKY46	DNA-binding protein 46	0.36	insig.
AT3G22800		leucine-rich repeat (LRR)/extensin	1.85	insig.
AT3G56400	WRKY70	WRKY DNA-binding protein 70	0.48	insig.
AT4G08950	EXO	phosphate-responsive 1 family protein	0.70	insig.
AT4G11280	ACS6	1-aminocyclopropane-1-carboxylic acid (ACC) synthase 6	0.47	insig.
AT4G24380		involved in 10-formyltetrahydrofolate biosynthesis	0.42	insig.
AT5G41750		disease resistance protein (TIR-NBS-LRR class) family	0.42	insig.
AT5G59550		zinc finger (C3HC4-type RING finger) family protein	0.63	insig.
AT5G64870		SPFH/Band 7/PHB domain-containing, flotillin	0.49	insig.
AT1G72900		Toll-Interleukin-Resistance (TIR) domain-containing protein	0.57	2.95
AT2G16660		major facilitator superfamily protein	0.52	1.30
AT2G34930		disease resistance family protein LRR	0.62	1.79
AT3G50930	BCS1	cytochrome BC1 synthesis	0.44	2.12
AT5G42380	CML37	calmodulin like 37	0.32	2.50